A Drug Cocktail of Rapamycin, Acarbose, and Phenylbutyrate Enhances Resilience to an Early-Stage Model of Alzheimer's Disease

Jackson Wezeman

A thesis

submitted in partial fulfillment of the

requirements for the degree of

Master of Science

University of Washington

2023

Committee:

Warren Ladiges

Thea Brabb

Brian Iritani

Jenna Klug

Program Authorized to Offer Degree:

Department of Comparative Medicine

University of Washington

Abstract

A Drug Cocktail of Rapamycin, Acarbose, and Phenylbutyrate Enhances Resilience to an Early-Stage Model of Alzheimer's Disease

Jackson Wezeman

Chair of the Supervisory Committee:
Warren Ladiges
Department of Comparative Medicine

The process of aging is defined by the breakdown of critical maintenance pathways leading to an accumulation of damage and its associated phenotypes. Aging affects many systems and is considered the greatest risk factor for a number of diseases. Therefore, interventions aimed at establishing resilience to aging should delay or prevent the onset of age-related diseases. Recent studies have shown a three-drug cocktail consisting of rapamycin, acarbose, and phenylbutyrate delayed the onset of physical, cognitive, and biological aging phenotypes in old mice. To test the ability of this drug cocktail to impact Alzheimer's disease (AD), an Adeno-Associated-Viral vector model of AD was created. Mice were fed the cocktail 2 months prior to injection and allowed 3 months for phenotypic development. Cognitive phenotypes were evaluated through a navigation learning task. To quantify neuropathology, immunohistochemistry was performed for AD proteins and pathways of aging. Age related lesions in the brain were evaluated through a geropathology grading platform. Results suggested the drug cocktail was able to increase resilience to cognitive impairment, inflammation, age-related lesions, and AD protein aggregation while enhancing autophagy and synaptic integrity, preferentially in female cohorts. In conclusion, female mice were more susceptible to the development of early stage AD neuropathology and learning impairment, and more responsive to treatment with the drug cocktail in comparison to male mice. Translationally, a model of AD where females are more susceptible would have greater value as women have a greater burden and incidence of disease compared to men. These findings validate past results and provide the rationale for further investigations into enhancing resilience to early-stage AD by enhancing resilience to aging.

Keywords: Aging, cognitive impairment, immunohistochemistry, drug cocktail, rapamycin, acarbose,

phenylbutyrate, Adeno-Associated-Viral vector, geropathology, resilience, Alzheimer's disease

Acknowledgements

I would like to thank my committee members Warren Ladiges, Thea Brabb, Brian Iritani, and Jenna Klug for their patience as this study was completed, the time each of them has made to meet with me, and their kind constructive criticism.

I would also like to thank the members of Ladiges Lab, who made themselves available for injections, necropsy, assays, and continuous discussions about results, sometimes at inconvenient times. I am incredibly lucky to have worked with such amazing and talented scientists.

I would like to give a special thanks to Warren Ladiges, who has mentored me throughout my higher education. It has been an incredible and fulfilling experience to participate in the lab.

Dedication

I would like to dedicate this work to my wife, who has supported me in numerous ways throughout graduate school, my sister, who is forever one of my most cherished friends, and my mom and dad, who have never once failed to tell me they are proud.

Table of Contents

Introduction……1

Materials and Methods……2

Results……5

Discussion……18

References……24

Introduction

Aging is a complex and multifaceted process arising from the breakdown of many necessary pathways. The aging process has thus been implicated as the greatest risk factor for the onset and development of "age-related diseases." While individual therapies may help to alleviate disease-specific phenotypes, a much broader and impactful focus is on aging itself. Zhang summarized it well stating, "The concept of geroscience is that since ageing is the greatest risk factor for many diseases and conditions, targeting the ageing process itself will have the greatest impact on human health" (Zhang 2023). Resilience aims to quantify biological aging and is defined as the ability to respond and recover from environmental stressors which disrupt homeostasis (Schorr 2018). Together, the geroscience concept and resilience could work to provide a platform to address aging and standardize evaluation and discovery toward age-related diseases. This study aims to examine the ability of resilience to delay the onset of Alzheimer's disease cognitive and neuropathology phenotypes.

To enhance resilience to aging, a multi-target approach may be helpful to address the many pathways of aging. Previous studies have examined a drug cocktail consisting of rapamycin, acarbose and phenylbutyrate for its impact on resilience (Zhou 2022). Rapamycin targets the mTOR pathway and has been known for its ability to extend lifespan in mice as well as reduce the presence of heart disease, inflammation, and cellular senescence, even with some already recommending it be used for clinical treatment of Alzheimer's Disease (AD) (Selvarani 2020). Acarbose is a regulator of glucose metabolism acting primarily in the intestine and targets alpha-glucosidase. Previous work in the field of Alzheimer's research has found dysregulation of glucose as an important modulator in the progression of the disease (Dewanjee 2022). The Intervention Testing Program (ITP) is an NIA program aimed at investing the anti-aging effects of different drugs. ITP studies demonstrated combinatorial effects between rapamycin and acarbose, finding together they had a greater affect than the individual drug (Strong 2022). Phenylbutyrate, while being used primarily for urea cycle disorders, modulates histone deacetylation and acts as a chaperone for proteins in the endoplasmic reticulum. In a recent trial for Amyotrophic Lateral Sclerosis (ALS), phenylbutyrate was shown to reduce functional decline in human patients (Paganoni 2020). When the drugs are combined into a drug cocktail, it was found not only to increase resilience to aging more than any combination of two or single drug, but it was also able to modulate aging in the brain and in main body organs (Zhou 2022, 2023).

Many murine models of Alzheimer's are unable to accurately simulate the onset and progression of the disease. One popular model, the 5xFAD mouse line, is a transgenic model using 5 amyloid precursor protein mutations to induce amyloid plaque formation in the brain. These mice, however, start developing pathology in the fetal stages. Not only does this remove the aging component from the brain but AD typically starts in humans around early to mid-life, far before cognitive phenotypes. To have better control over and to monitor the process of onset of disease phenotypes, an adeno-associated-viral (AAV) vector model was created expressing human amyloid beta-42 (Aβ-42) peptide, and P301L tau, a human mutated sequence of tau protein. There are several major advantages to this model. First, disease progression can be modeled in aging mice. Because the vector is able to be administered to mice of any age, the aging neuropathology of these mice can be allowed to interact with induced expression of these proteins for a much more translational model. Second, control of the onset additionally allows for the researcher to have greater control experimentally to assess how diet, environment, or other factors affect the induced changes. This means the model can be adapted to a number of experiments. Lastly, the landscape of AD research has begun to focus on how to treat early stages of the disease and how to prevent its onset. The control in creating a model capable of simulating the beginning stages of disease progression opens the door for development of therapies at these stages and strengthens translational value.

This study propositions that increasing resilience to aging through a drug cocktail of rapamycin, acarbose, and phenylbutyrate will delay or prevent the onset and/or progression of AD neuropathology and cognitive impairment in an AAV vector model of AD. Aim 1 of this study was designed to characterize cognitive impairment and body composition phenotypes present between mice given medicated and non-medicated diets as well as AD and SHAM infected cohorts. Aim 2 was designed to characterize the changes in neuropathology and age-related lesions in the brains of mice to determine the ability of the AAV vector to simulate characteristic AD neuropathology, and the effect of the drug cocktail in modulating it.

Materials and Methods

Mice. This study used 80 male and 80 female 22-month-old C57BL/6J mice. Forty males were selected at random to receive a medicated diet consisting of rapamycin, acarbose, and phenylbutyrate with the remaining forty males receiving non-medicated feed. The females were similarly separated. Cohorts of twenty mice were formed from ten medicated fed mice and ten non-medicated fed mice, separated by sex. After 2 months of treatment, mice were infected with AAV-AD or AAV-SHAM vector, to which the primary researcher was blinded. After an additional 5 months, when mice were 27 months of age, end-of-study assays were performed followed by carbon dioxide (CO_2) asphyxiation. Brains were immediately harvested and sectioned along the midsagittal plane into left and right halves, which were then immersed in 10% neutral buffered formalin (NBF) and allowed to fix for 72 hours before being transferred to 70% ethanol. The left sagittal hemispheres of the brain were then submitted to Alzheimer's Disease Research Core – Neuropathology Lab at Harborview Hospital in Seattle, Washington where they were processed for paraffin embedding, serially sectioned at 5 µm into coronal slices, and stained with hematoxylin and eosin (H&E) and Luxol Fast Blue (LFB) for histologic examination. The main body organs were trimmed such that sections were both fixed and flash frozen. The right sagittal hemisphere was flash frozen.

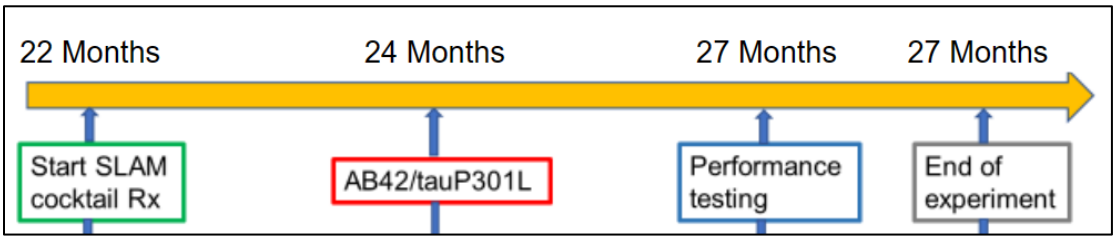

Figure 1. Experimental timeline. All cohorts followed this timeline and were separated by at least one week.

Diet. The medicated repelleted rodent chow diet contained 14 ppm encapsulated rapamycin, 1000 ppm acarbose, and 1000 ppm phenylbutyrate. The non-medicated diet consisted of only repelleted regular chow. Each drug was delivered to Test Diet Inc. (Indiana, USA) where both diets were produced. Upon arrival the diets were refrigerated and each week the diet was replaced in the cage to ensure quality. Food intake was monitored to determine the amount of food ingested. Intake was calculated each week by comparing the initial weight of food supplied to each cage to the final weight of food leftover. The consumption for each mouse was averaged across the cage. Mice were fed ad libitum.

Vector. An AAV vector delivery system was used to induce expression of Aβ-42 and P301L tau in mouse neurons. This AAV vector is a non-replicating DNA parvovirus that has a specially designed capsid known as AAV PHP.eB, which is a subvariant of AAV9, engineered specifically to have an affinity for neurons. This variant crosses the blood brain barrier through the receptor LY6A. Subvariant AAV PHP.eB targets a specific isoform of the LY6A

receptor present in significant numbers only in C57BL/6 mice. Other mouse strains do not let the virus into the brain Mathiesen 2020). There are three different constructs in total (Table 1). One induces expression of human Aβ-42, one induces P301L, a human mutated tau known to instigate AD tau pathology, and one induces Cherry, a nonsense protein. The Aβ-42 vector uses the EF-1a promoter, contains a BRI sequence to anchor the protein in the cell membrane, and contains a GFP tag for reporting. The tau vector uses the CAG promoter. The cherry vector uses the hSyn promoter.

cDNA Sequence	Promoter	Additional Sequence	Reporter
Human Aβ-42	EF-1a	BRI membrane anchor	Green Fluorescent Protein (GFP)
P301L-Tau (FTD)	CAG	N/A	N/A
Cherry (Nonsense)	hSyn	N/A	N/A

Table 1. The contents of each construct including cDNA sequence, promoter, additional sequences, and reporters. Only the Aβ-42 construct has a reporter.

The concentration of the injected AD vector was 5 x 10^{11} Genome Copies (GC) for both the Aβ-42 and tau constructs while the SHAM vector concentration was 1 x 10^{12} GC for the cherry construct. The prepared vector was diluted with sterile filtered PBS such that each dose was 80 µl for each administration. Mice were under isoflurane anesthesia for 10 minutes before administration of the vector retro-orbitally and placed into a recovery cage immediately after. Retro-orbital administration was chosen for its low lethality rate and its ability to transduce the entire brain, in comparison to other methods such as trans-cranial and intranasal, where transduction is specific to the region injected or occipital bulb, respectively (Konno 2020, Mathiesen 2020, Hu 2021).

QMR. Quantitative Magnetic Resonance Imaging (QMR) utilizes magnetic resonance capability in biological tissues to quantify fat and lean tissue. The machine is standardized using canola oil standard of known fat. Mice are placed in a specialized plastic tube and inserted into the machine. One scan takes 50 seconds. Three scans are completed and averaged to ensure accuracy. QMR was performed once prior to infection with the vector and once again at endpoint.

Box Maze. Box Maze is a spatial navigation learning task developed to test cognitive function in mice (Darvas 2020). The maze consists of a rigid plastic box with 7 dud escape holes and 1 true escape hole leading to a dark empty cage. The box is lined with a reflective lining and a light is shined over the box to create a mild stressor. To start the evaluation mice are placed in the center of the maze and allowed 120 seconds to solve the maze. If the time is exceeded, mice are guided toward the exit. Once the mice are in the escape cage and the 120 seconds of the trial have passed, the mouse is returned to the home cage for 2 minutes and the process is repeated for 4 trials. It is expected mice with cognitive impairment will have longer average escape times.

Immunohistochemistry. Brains were randomly selected high performing and low performing box maze mice representing each of the four sex/diet cohorts. This totaled 14 male and female non-medicated mice and 15

male and female medicated mice to be stained for neuropathology. Brains were stained on 4-5 µm sections with an Abcam kit (HRP/DAB Rabbit Kit: ab64261, HRP/DAB Mouse Kit: ab64259). Slides were first hydrated in xylene, 100% ethanol, 95% ethanol, 70% ethanol, and water followed by antigen retrieval by citrate buffer pH 6 or Tris-EDTA pH 9. The slides were allowed to cool at room temperature. Once cool, a hydrophobic barrier was drawn, and the slides were washed in TBST for 5 minutes. Next, the slides were incubated with a peroxidase block for 10 – 30 minutes, washed three times for 5 minutes, incubated with a protein block for 10 – 30 minutes, washed three times for 5 minutes, and incubated overnight at 4^{o}C with primary antibody diluted in TBST. Slides were washed with TBST three times for 5 minutes, incubated with secondary antibody for 10 – 30 minutes, washed three times for 5 minutes, incubated with streptavidin for 10 – 30 minutes, washed three times for 5 minutes and incubated for 30 – 150 seconds with DAB Chromogen. After three water washes for 3 minutes, the slides were dehydrated in 70% ethanol, 100% ethanol, and xylene before having slide covers mounted with hydrophobic mounting media. The primary antibodies used are as listed: 1/1500 GFP (Abcam: ab290), 1/1000 IBA1 (Abcam: ab178846), 1/500 H31L21 (Invitrogen: 700254), 1/100 HT7 (Invitrogen: MN1000B), 1/(250 or 300) Synaptophysin (Novus: NBP2-25170), 1/200 yH2AX (Proteintech: 10856-1-AP), 1/800 MCP-1 (Novus: NBP1-07035), 1/250 PSD95 (Abcam: ab18258), 1/200 ATG5 (Invitrogen: MA5-35339), 1/2000 GFAP (Invitrogen: PA1-10019). HT7 was the only anti-mouse antibody used and a mouse-on-mouse blocking agent (Invitrogen: R37621) was applied for 30 minutes post protein block washes to reduce noise from secondary antibody binding and an additional three 5-minute washes were added before primary antibody incubation. Listing time ranges and two different antigen retrievals are to account for variation needed in fine-tuning the IHC protocol to specific antibodies. Synaptophysin was the only antibody where two concentrations were used. Non-medicated mice were stained at 1/250 while medicated cohorts were stained at 1/300. This was done due to accessibility of primary antibody. Since it was expected medicated cohorts would have greater expression of synaptophysin, they were chosen for the 1/300 dilution.

Image Processing. Digital image analysis was performed on IHC-stained slides at 200x magnification lens using the NIS-D microscope software package (Nikon Instruments Inc.). For density measurements ImageJ was used. ImageJ is an open-source image processing software package (https://imagej.net/downloads, version 1.54d). An object-based approach to quantification was used to identify positive staining based on a binary approach consisting of present/absent DAB intensity. Images first had their background subtracted before adjusting contrast and brightness values to only include positive (present) staining. Once done, measurement options allowed for the percentage of the area in the photo represented to be recorded as percentage values. For all neuropathological evaluation, only hippocampus regions of each mouse were analyzed. Density was chosen primarily to identify range of spread specifically in the context of spatial patterns of pathology.

Geropathology. H&E-Luxol Fast Blue slides were obtained from the Alzheimer's Disease Research Core – Neuropathology Lab at Harborview Hospital in Seattle, Washington and were graded for age-related lesions and pathology in a blinded manner by board-certified pathologists (Jenna Klug, Jessica Synder). A composite lesion score (CLS) was calculated by adding the severity score of age-related lesions in the brain for each mouse in a cohort, adding the total lesion score for all mice in each specific cohort and dividing by the number of mice in the cohort were summed and used as the analysis value (Snyder 2019). Age-related lesions were graded based on six categories of lesions (Figure 2)(Tarrant 2020, Ward 2022).

Age-Related Lesion	Score	Description
Tumor	0	absence of tumor
	1	presence of benign tumor
	2	presence of extensive or multiple benign or malignant tumor(s).
Vacuolation	0	No lesions
	1	minimal cytoplasmic vacuolation of neurons (usually clear or pale eosinophilic), neuropil, white matter
	2	mild vacuolation changes
	3	moderate vacuolation changes
	4	severe vacuolation changes
Inflammation	0	No lesions
	1	minimal lesions
	2	mild lesions
	3	moderate lesions
	4	sever elesions
Thalamic Mineralization	0	No lesions
	1	Presence of mineral deposits
Brainstem Mineralization	0	No lesions
	1	Presnce of Mineral Deposits
ICIBS	0	No lesions
	1	Hrano-like neuronal inclusions within the thalamus, consisting of 2 x 4 to 8 um eosinophilic, refractile cytoplasmic inclusions that vary in sheep from oval to rod-shaped and angular

Figure 2. Geropathology scoring rubric for mouse brains. Scoring is designed to be summative.

Statistics

For differences between cohorts, one-way ANOVA was used to assess significance. For comparison of means between two groups, Fischer's t-test was used. For correlations, Pearson's coefficients were determined to have strong correlations if the coefficient was less than -0.5 or greater than 0.5. All statistics, p-values, and graphs represented were generated in GraphPad Prism version 10.1.0. Outliers were determined by (1.5 x IQR) further than the third or second quartile. Significance was determined at $p < 0.05$.

Results

Mice infected with AAV-Ab42/ptau maintained body weight similar to mice infected with AAV-SHAM.
Weekly weights were used to calculate body weight between baseline and endpoint. Body fat mass was measured by QMR and performed prior to injection and again at endpoint. Food consumption was monitored weekly and the last four weeks of the study, when consumption had stabilized. Female mice infected with AAV Aβ-42/pTau (AAV-AD) and treated with the drug cocktail had a significant loss in weight (Figure 3A), while drug cocktail treated male mice with AAV-AD and AAV-Sham lost weight (Figure 3B). When comparing loss of fat, all female cohorts except the medicated AAV-SHAM demonstrated a significant decrease in fat (Figure 3C). Only the male non-medicated AAV-SHAM cohort had a statistically significant loss in fat (Figure 3D). In comparison of the male and female cohorts, it does appear male mice lost more weight in contrast to female mice who lost more fat. For the consumption of food, both male and female medicated cohorts consumed more food per mouse than mice in non-medicated cohorts (Figure 3E-3F). Interestingly, the medicated female AAV-SHAM cohort consumed more food on average in comparison to the medicated AAV-AD cohort, which led to a lower average weight loss for the AAV-SHAM cohort, possibly alluding to a dose-dependent response to the drug cocktail. Overall, though there was a sex-dependent trend in the distribution of weight loss, both male and female cohorts-maintained weight between AAV-AD and AAV-SHAM cohorts of the same feed.

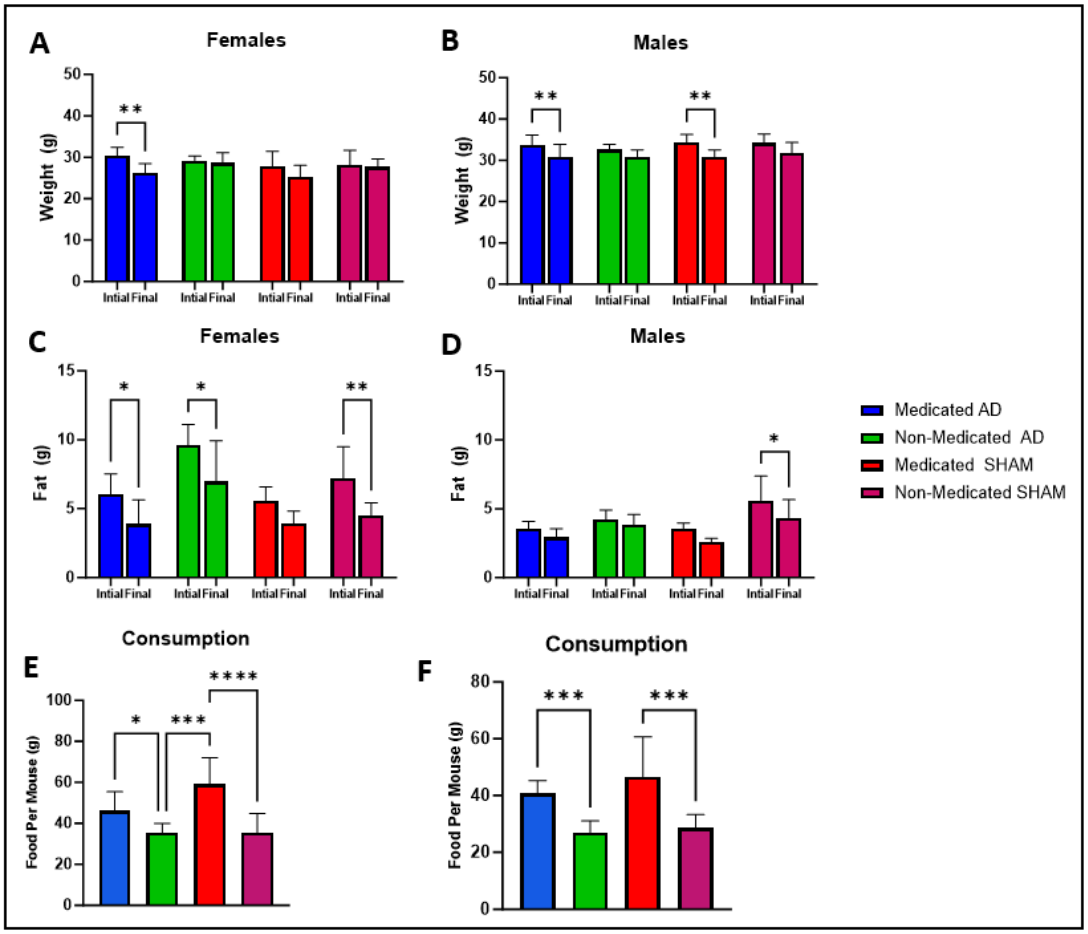

Figure 3. Body weight and food consumption for experimental cohorts. (A) The female medicated AAV-AD cohort lost significantly more weight compared to baseline. (B) The male medicated cohorts lost significantly more weight compared to baseline. (C) All female cohorts except medicated AAV-SHAM mice lost significant amounts of fat in comparison to pre-injection. (D) Only male non-medicated AAV-SHAM mice lost a significant amount of fat from injection to endpoint. (E) Female medicated cohorts consumed significantly more food than non-medicated cohorts. (F) Male medicated cohorts consumed significantly more food than non-medicated cohorts. n = 5-8. * = $p \leq 0.05$, *** = $p \leq 0.001$, **** = $p \leq 0.0001$.

The drug cocktail reduced cognitive impairment in female mice.

The Box maze is a spatial navigation learning task in which mice are given 4 trials to escape the maze as quickly as possible. Each trial allowed for separation of fast and slow performers based on improvement of escape times by non-medicated AAV-SHAM mice, which served as the control. Trial 2 was selected for the female cohorts as the female control cohort continually improved their times with Trial 2 having the greatest change in escape time. Trial 3 was selected for the male cohorts as it was the last trial to mark an improvement of the control cohort on escape time. For the female cohorts, the medicated AAV-AD mice performed faster than the non-medicated AAV-AD mice regardless of injection and even when separated based on performance (Figure 4A, 4C). In male cohorts, while the non-medicated AAV-SHAM cohort had the fastest escape times, both cohorts of fast medicated mice performed faster than the fast non-medicated AAV-AD cohort (Figure 4B, 4D).

The Box maze data suggests a reduction in cognitive impairment for female cohorts based on small differences in fast groups and larger differences in slow groups. It was also seen that slow AAV-AD cohorts performed worse than slow AAV-SHAM cohorts. As for the male cohorts, not only did they perform slower than the female mice, but the differences in improvement were also much smaller, suggesting more severe cognitive impairment than females. It was seen that in fast groups, AAV-AD mice performed worse than AAV-SHAM mice. These results point to a rescue of cognitive impairment in female cohorts with a smaller impact on male cohorts.

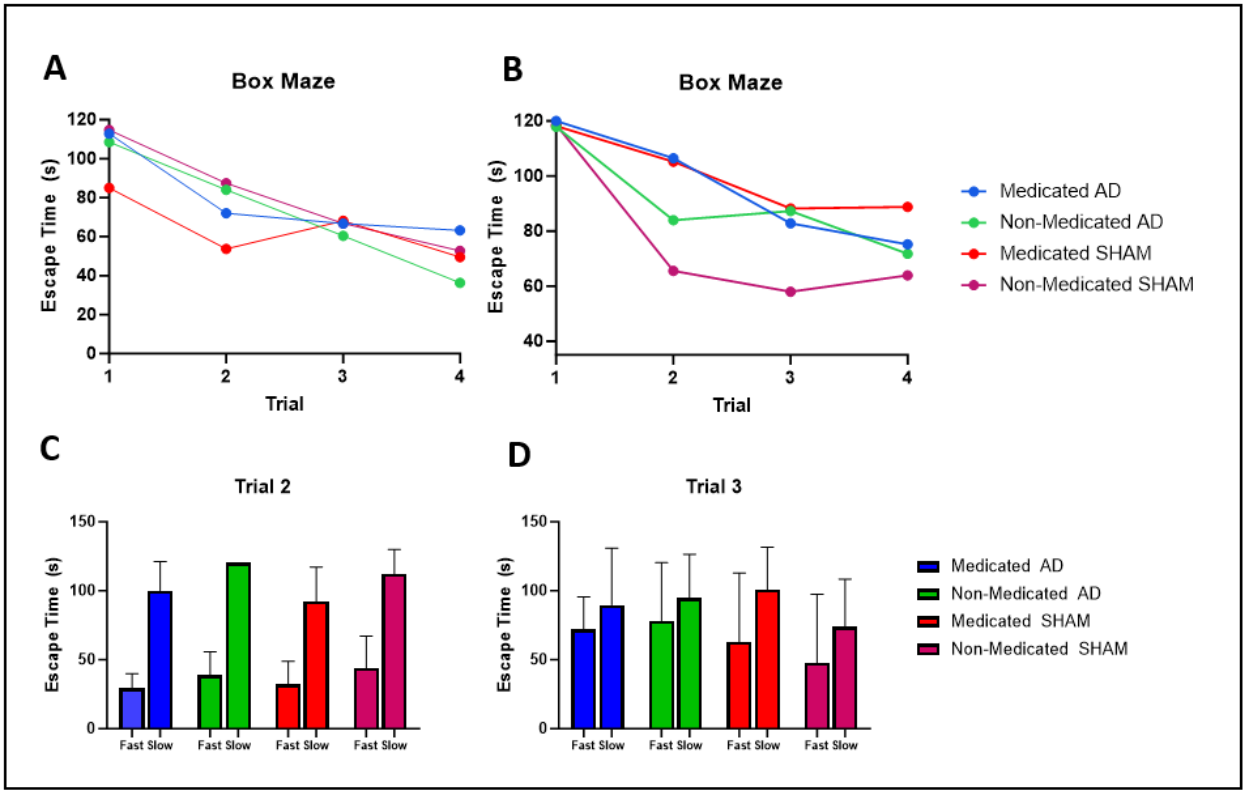

Figure 4. Assessment of cognitive phenotype. (A) Medicated cohorts had faster escape times than non-medicated cohorts in trial 2. (B) Male medicated cohorts performed slower than non-medicated cohorts in trial 2. (C) Separation of fast and slow performers for each female cohort for trial 2. Medicated cohorts outperform non-medicated cohorts in fast and slow separated groups. (D) Separation of fast and slow performers for each male cohort for trial 3. Non-medicated AAV-SHAM mice outperformed all other cohorts. Fast medicated cohorts performed faster than the fast non-medicated AAV-AD cohort. n = 5-8.

The drug cocktail suppressed expression of Aβ-42 in the hippocampus of female mice infected with the AAV-AD vector.

Histopathological assessment of the brain focused on the hippocampus as the sub anatomic region of interest for its translational relevance as the primary learning and memory center adversely affected by AD in human patients. Following IHC, quantification was performed using ImageJ, an image-focused research software package, using images taken of DAB-Chromogen-stained brains. To quantify staining, density was calculated by highlighting positive pathology and measuring the “percent area” highlighted in the image. Green fluorescent protein (GFP) was used as a reporter sequence in the Aβ-42 viral construct to validate the presence of the AAV vector in neurons. IHC using an optimized anti-GFP antibody was employed. In female and male cohorts, significant differences were observed between AAV-AD and AAV-SHAM infected mice (Figure 5A, B). No differences in densities of GFP were seen between medicated and non-medicated AAV-AD cohorts for both sexes suggesting the drug cocktail did not interfere with viral-mediated transduction.

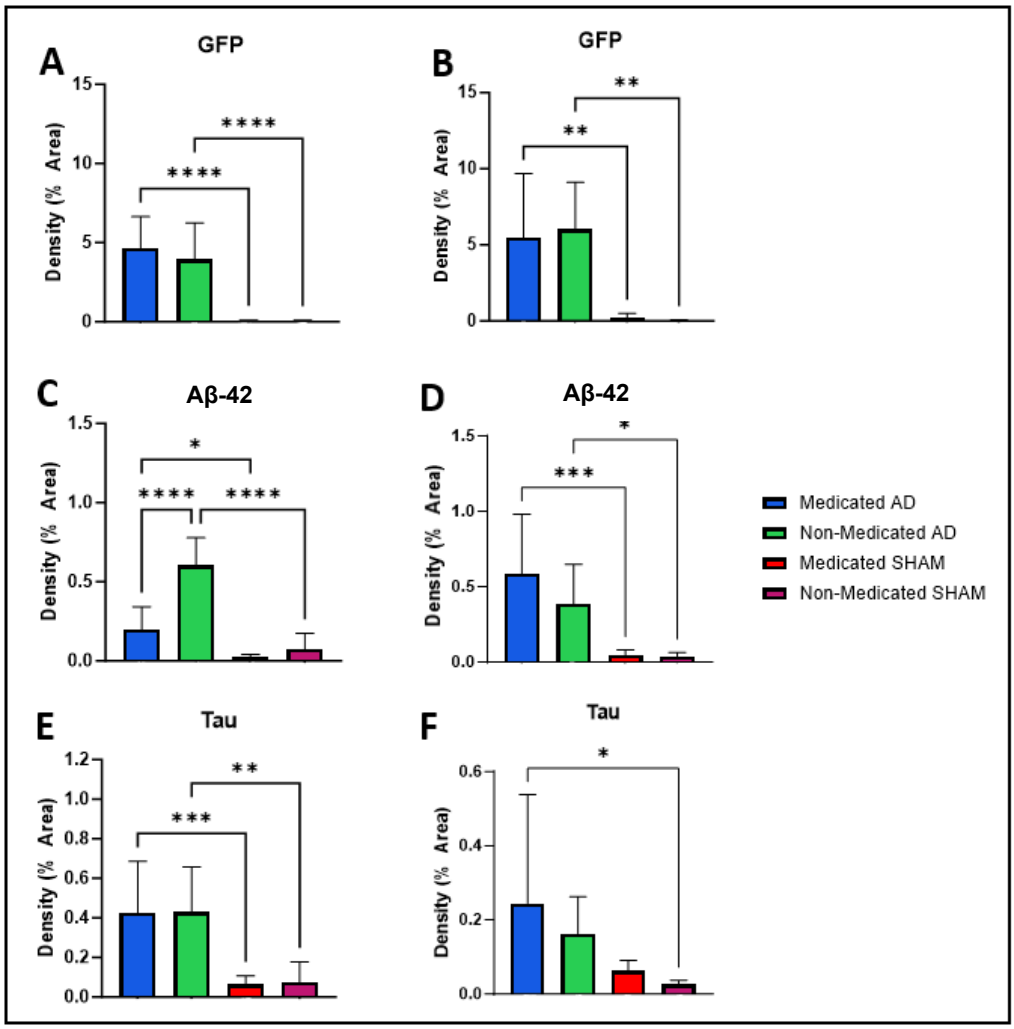

Figure 5. AAV-AD induced proteins GFP, Aβ-42, and tau in the hippocampus quantified in ImageJ by area density of DAB. GFP is a reporter gene for the Aβ-42 construct. Aβ-42 was stained with H31L21 which is specific for the sequence. Tau was stained by HT7 which is specific for human tau. (A-B) Both females and males had no difference between AAV-AD cohorts but significant differences between AAV-AD and AAV-SHAM infected cohorts. (C-D) Equivalent comparisons to Figure A and B, show similar trends with AAV-AD cohorts expressing significantly more Aβ-42 than AAV-SHAM cohorts. Female medicated AAV-AD mice did show a significant decrease in the density of Aβ-42 when compared to the non-medicated AAV-AD cohort. (E-F) Female cohorts in similar comparisons to Figure A and B saw similar results with AAV-AD cohorts expressing more tau than AAV-SHAM cohorts. Male cohorts saw higher averages for AAV-AD cohorts but only the medicated cohort was significant against the non-medicated AAV-SHAM cohort. n = 5-8. * = $p \leq 0.05$, ** = $p \leq 0.01$, *** = $p \leq 0.001$, **** = $p \leq 0.0001$.

As expected, expression of Aβ-42 reflected trends seen in densities of GFP. For both males and females, AAV-AD cohorts had significantly greater expression of Aβ-42 in comparison to AAV-SHAM cohorts. (Figure 5C-5D). More importantly, the female medicated AAV-AD mice had significantly less Aβ-42 expression compared to the non-medicated AAV-AD. Female AAV-AD cohorts also had significantly greater expression of tau in comparison to AAV-SHAM cohorts. No decrease in expression of tau was observed between AAV-AD cohorts (Figure 5E). While not significant against female cohorts, male expression of tau for AAV-AD infected mice was lower than female AAV-AD cohorts. While averaging higher, only medicated AAV-AD mice were significant against AAV-SHAM non-medicated mice (Figure 5F). Many males infected with the AAV-AD vector had density levels similar to AAV-SHAM

infected mice. It is possible male mice may not be as susceptible as female mice to the accumulation of AD proteins as male mice appear to have less expression overall, with similar expression of GFP.

Figure 6 shows characteristic structures of AAV-AD expressed proteins in the hippocampus. Figures 6A-6C are of GFP expression, Figures 6D-6F are of Aβ-42, and Figures 6G-6I show tau expression. For each set of three images: first is an AAV-SHAM infected mouse, second is AAV-AD infected mouse, and third is a close-up of an AAV-AD infected neuron showing positive staining. In all AAV-SHAM images, no density is observed. In all AAV-AD images, examples of positive stain are circled in red. Of those circles, one has been selected for the close-up. Each enlarged figure demonstrates intercellular expression of relevant proteins and the spreading of those proteins down the axon.

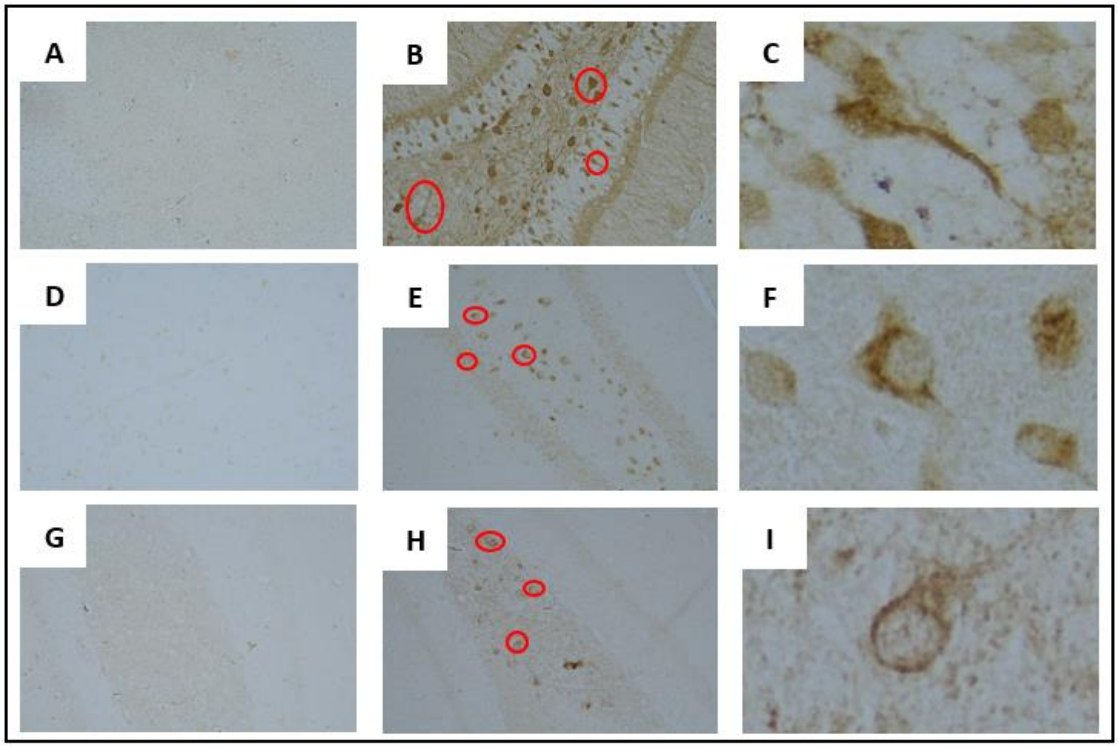

Figure 6. Images of immunohistochemistry stains to visualize AAV-AD protein expression in the hippocampus taken at 20x. Positive stains have annotations highlighting examples of positive staining. (A-B) Characteristic density of GFP in AAV-SHAM and AAV-AD infected mice, respectively. (C) Enlarged image of GFP positive neuron. (D-E) Characteristic density of Aβ-42 in AAV-SHAM and AAV-AD infected mice, respectively. (F) Enlarged image of Aβ-42 positive neuron. (G-H) Characteristic density of human tau in AAV-SHAM and AAV-AD infected mice respectively. (I) Enlarged image of human tau positive neuron.

The drug cocktail altered aspects of neuropathology and concentration of non-neuronal cells in the hippocampus of mice.

Because synaptic integrity is one of the first processes damaged in AD resulting in cognitive impairment, synaptic markers were analyzed in the hippocampus. Two targets were chosen, one for presynaptic integrity and one for postsynaptic integrity evaluation. Synaptophysin was chosen for its role in pre-synaptic vesicle release. PSD-95 was chosen for its role in regulation and organization of synapses. Female medicated cohorts had greater expression of synaptophysin in comparison with non-medicated cohorts with the same vector (Figure 7A). In addition, female AAV-AD cohorts had on average less synaptophysin expression in comparison to AAV-SHAM cohorts. While synaptophysin expression for the male medicated AAV-AD cohort was higher than the non-medicated AAV-AD cohort, greater differences were seen between the medicated AAV-SHAM cohort and non-

medicated AAV-SHAM cohort (Figure 7B). In post-synaptic marker PSD-95 female cohorts had a slightly greater expression in medicated cohorts, while male medicated cohorts had slightly less expression than non-medicated cohorts (Figure 7A-7B). This data suggests the drug cocktail enhances synaptic integrity in female cohorts and pre-synaptic integrity in male cohorts. In addition, it also suggests mice infected with the AAV-AD vector have a reduction in synaptic integrity in comparison to their AAV-SHAM counterparts.

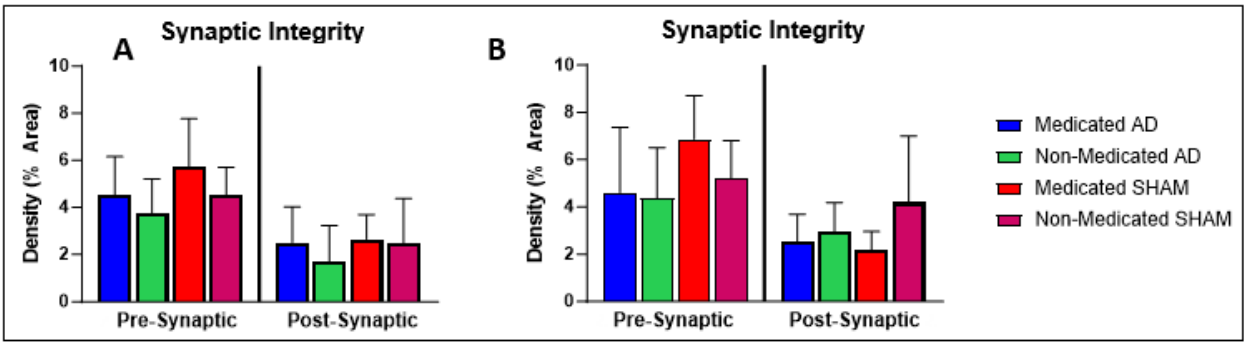

Figure 7. Density of characteristic markers of synaptic health in the hippocampus quantified using ImageJ. (A) Female cohorts saw higher density of synaptophysin in medicated cohorts and a decrease in synaptophysin in AAV-AD infected cohorts. A slight increase in density was observed for PSD-95 in medicated mice. (B) Male cohort saw an increase in density of synaptophysin in medicated cohorts and an overall decrease in AAV-AD infected cohorts. No differences were observed in PSD-95. n = 5-8.

Figure 8 shows IHC images of staining done for pre-synaptic and post-synaptic proteins. Figure 8A demonstrates positive staining for synaptophysin with Figure 8B showing an enlarged image. Synaptophysin is expressed in the axon and appears clustered and follicular due to its direct involvement with vesicle membranes. Figure 8C demonstrates positive staining for PSD-95 with Figure 8D showing an enlarged image. PSD-95 is expressed closer to the cell body where excitatory neurons are located. PSD-95 acts as a structural mediator for bringing membrane proteins and relevant signals together. It also appears follicular, as demonstrated by small cavities of DAB staining.

These results suggest the drug cocktail influences presynaptic integrity in both males and females while in AAV-AD infected mice, expression of synaptophysin is decreased. Post-synaptic integrity seems to be affected in AAV-AD cohorts for female mice but is less affected in male medicated cohorts. The sex differences in post-synaptic integrity appear to mirror expression of AAV-AD induced protein expression. This suggests, post-synaptic integrity may be more closely linked to AD neuropathology than pre-synaptic integrity in the early stages.

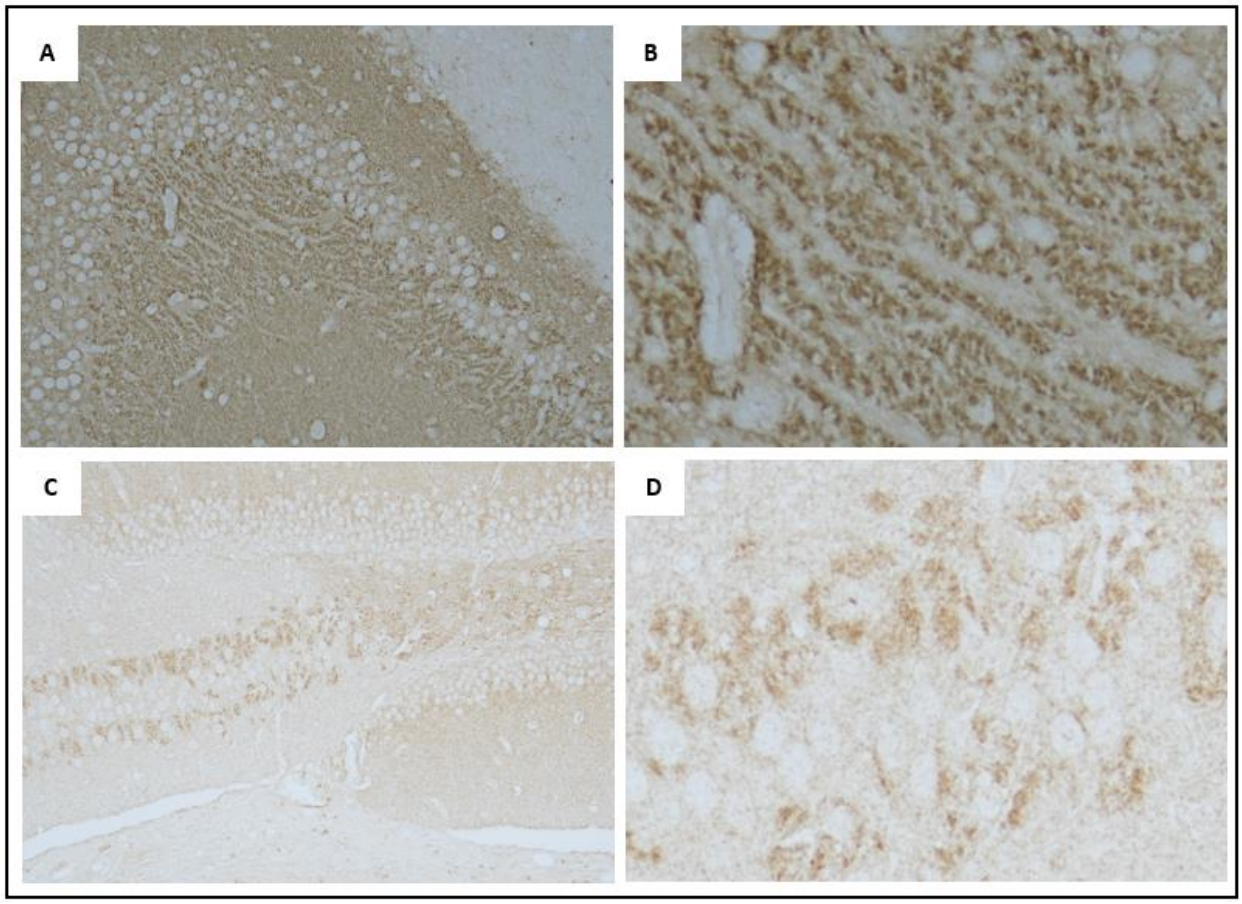

Figure 8. Images are representative of the characteristic markers of synaptic integrity in the hippocampus. (A) 20x image of the hippocampus. Stained for Synaptophysin. (B) Enhanced image of 8A (C) 20x image of the hippocampus. Stained for PSD-95. (D) Enhanced image of 8C.

As Ab42 and Tau expression progresses, accumulation of excess unwanted protein can lead to signals for inflammation, increases in the amount of DNA damage, and an increase in autophagy (Currais 2017, Ainslie 2021). These pathways were analyzed by IHC in the hippocampus. MCP-1 is a signal for inflammation and acts as a recruiter of additional inflammatory factors. yH2AX is a signal for DNA damage response and is upregulated in the presence of double-stranded DNA breaks. ATG5 is a marker for autophagy and is important for destruction of damaged cellular components.

In general, female AAV-AD mice, with or without drug cocktail treatment, had higher expression of representative markers in comparison to their AAV-SHAM cohorts. In addition, medicated cohorts had lower expression than non-medicated cohorts though not significant (Figure 9A). In male cohorts the same trends with AAV-AD medicated and AAV-AD non-medicated mice were observed against their counterparts, as well as the same trend between medicated and non-medicated cohorts (Figure 9B). More specifically, both medicated and non-medicated female AAV-AD cohorts had significantly higher expression of yH2AX in comparison to the non-medicated AAV-SHAM cohort. In addition, compared to their non-medicated counter parts, medicated cohorts had on average a lower density of yH2AX (Figure 9A). Male cohorts mirrored significantly less density of yH2AX in the medicated AAV-AD compared to the non-medicated AAV-AD cohort. Non-medicated AAV-AD mice also had significantly denser yH2AX than medicated AAV-SHAM mice (Figure 9B). Males did not have the same cocktail treatment trends, as only the medicated AAV-AD cohort had less density than its non-medicated AAV-AD

counterpart. No significant differences in female cohorts were observed in evaluation of autophagy. Male cohorts saw a significant decrease in expression between the medicated AAV-AD compared to the non-medicated AAV-AD cohort. While not significant, the medicated AAV-SHAM also had less dense expression compared to the non-medicated AAV-SHAM cohort (Figure 9B).

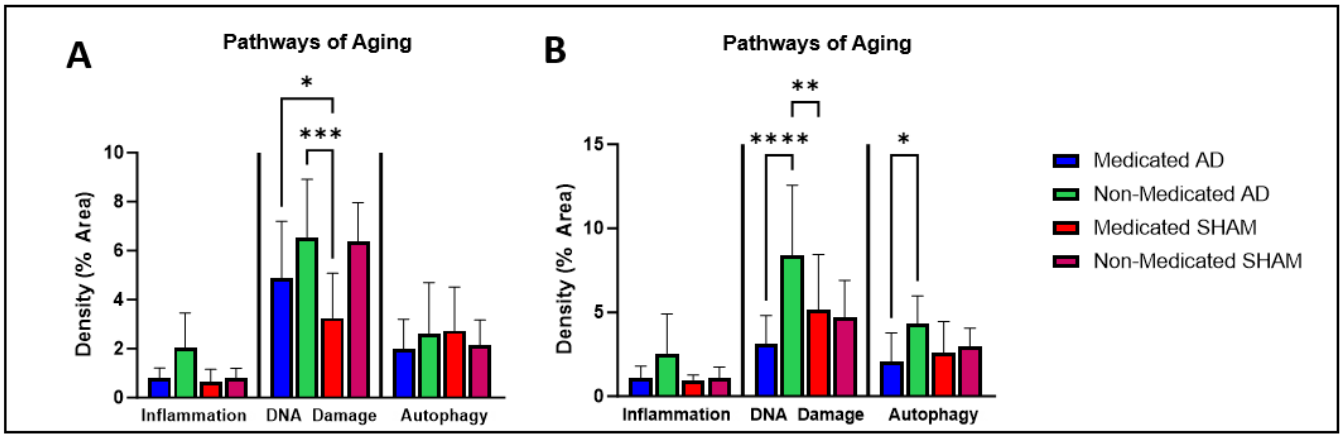

Figure 9. Density of IHC staining for characteristic markers of pathways of aging in the hippocampus. (A) Female AAV-AD infected mice had higher densities of MCP-1 in comparison to AAV-SHAM infected mice, as well as medicated cohorts having lower densities than their counterparts. Female AAV-AD infected mice had increased density of γH2AX compared to medicated AAV-SHAM infected mice. On average, medicated cohorts had lower densities than their non-medicated counterparts. No trends were observed for ATG5 in female mice. (B) Male AAV-AD infected mice had higher densities of MCP-1 in comparison to AAV-SHAM infected mice, as well as medicated cohorts having lower densities than their counterparts. Male non-medicated AAV-AD infected mice had increased density of γH2AX compared to medicated AAV-SHAM and AAV-AD infected mice. On average, medicated cohorts had lower density compared to non-medicated cohorts. Male medicated cohorts on average had lower density of ATG5 in comparison to non-medicated cohorts, with a significance decrease between AAV-AD infected cohorts. n = 5-8. * = $p \leq 0.05$, ** = $p \leq 0.01$, *** = $p \leq 0.001$, **** = $p \leq 0.0001$. Aging pathway biomarkers: MCP-1 for inflammation; γH2Ax for DNA damage response; ATG5 for autophagy.

Figure 10 shows images of IHC staining for inflammation, DNA damage response, and autophagy. Figure 10A demonstrates positive staining for MCP-1 with Figure 10B showing an enlarged image. MCP-1 is made in the cytoplasm and released extracellularly as a chemokine, thus evidence of staining inside and outside neurons. Figure 10C demonstrates positive staining for γH2AX which acts on histone targets recruiting additional proteins to initiate a DNA damage response. It is localized in the nucleus and recognized as a “polka-dot“ pattern. Figure 10D shows an enlarged image. Figure 10E demonstrates positive staining for ATG5 with Figure 10F showing an enlarged image. ATG5 can be localized to the nucleus but is primarily expressed in the cytoplasm where it forms complexes necessary for phagosomes. Thus locational expression can be apparent in the axons of the neuron and outside the nucleus.

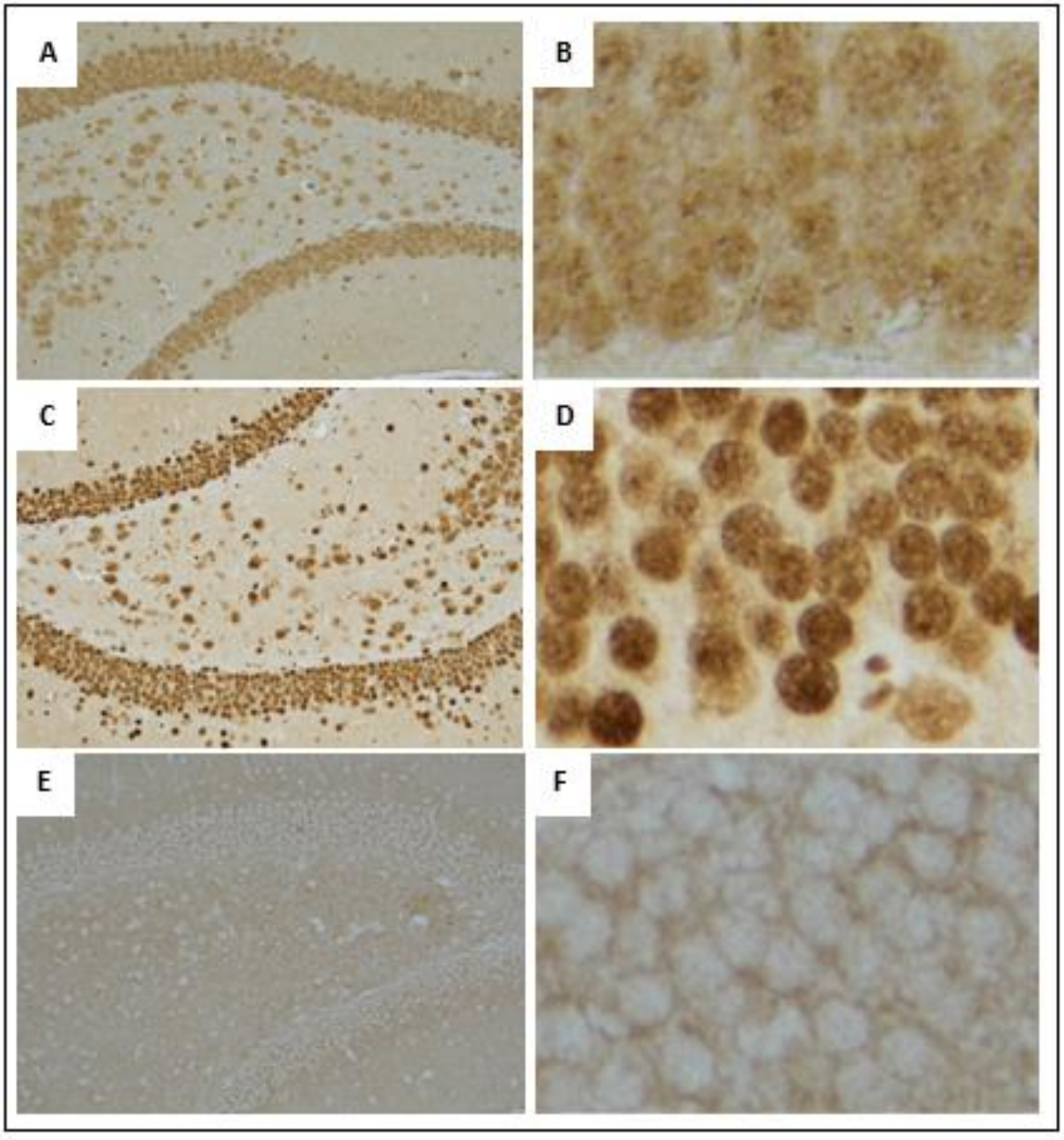

Figure 10. Images are representative of the characteristic markers of aging pathways in the hippocampus. (A) 20x image of the hippocampus. Stained for MCP-1. (B) Enhanced image of 10A. (C) 20x image of the hippocampus. Stained for yH2AX. (D) Enhanced image of 10C (E) 20x image of the hippocampus. Stained for ATG5. (F) Enhanced image of 10E.

The expression of these markers demonstrates cocktail mediated responses to inflammation and DNA damage. For both sexes, differences in inflammation between cohorts mirrored differences in DNA damage and for males, differences in autophagy. This suggests specific responses to expression of Aβ-42 and Tau, which are alleviated by the drug cocktail.

The role of non-neuronal cells in the progression of AD is significant. Microglia responses can become increased to the point of synapse engulfment and development of tau pathology (Hansen 2018). Astrocytes help in neuronal maintenance of synapses and clearing of debris but have been implicated in being activated by microglia and contributing to inflammation during AD (Orre 2014). IBA1 is a marker for activated microglia and GFAP is a marker for activated astrocytes. Surprisingly, both female medicated AAV-AD and medicated AAV-SHAM cohorts had significant increases in IBA1 expression in comparison to the non-medicated AAV-SHAM cohort. Both cohorts also had increased expression compared to the medicated AAV-AD cohort (Figure 11A). In direct contrast, for male cohorts there were no differences in IBA1 staining density except that all cohorts had significantly less IBA1 expression in comparison to the non-medicated AAV-AD cohort. It appeared on average that AAV-AD cohorts had higher expression of IBA1 than AAV-SHAM cohorts (Figure 11B). In both medicated AAV-AD and AAV-SHAM female cohorts there was a significant increase in GFAP expression than in both non-medicated cohorts (Figure 11A). Male cohorts did not follow this trend. In males, AAV-AD cohorts on average had higher expression of GFAP in comparison to AAV-SHAM cohorts. Microglia activate astrocytes and sex differences have been observed in astrocyte activation (Crespo-Castrillo 2020, Posillico 2021), which may explain the differences in non-medicated cohorts. This suggests the drug cocktail impacted astrocyte activation preferentially in female cohorts, and potentially given the intensity of the male response, in male cohorts.

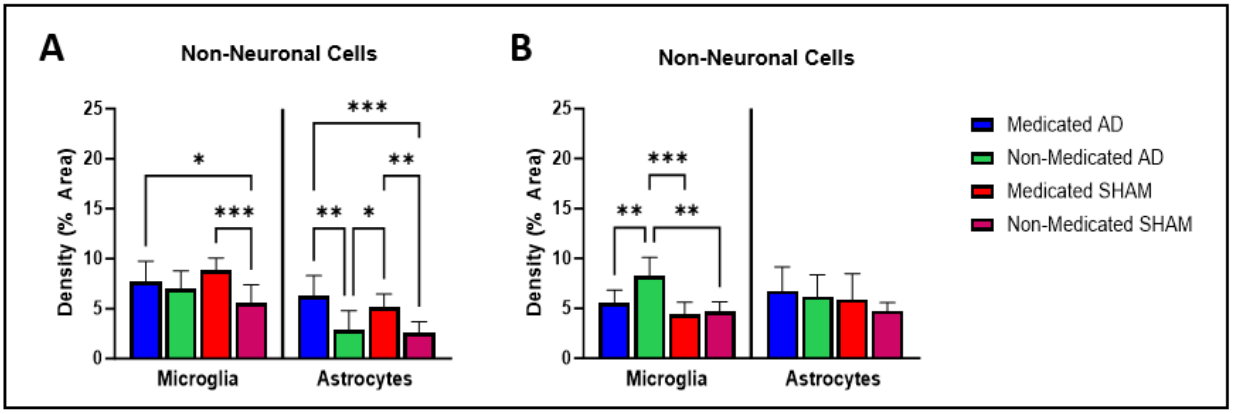

Figure 11. Density of IHC staining for non-neuronal cells in the hippocampus. (A) Female medicated AAV-AD and AAV-SHAM cohorts had significantly higher IBA1 density than the non-medicated AAV-SHAM cohort and higher densities compared to the non-medicated AAV-AD cohort. Both medicated AAV-AD and medicated AAV-SHAM cohorts had high densities of GFAP in comparison to both the non-medicated AAV-SHAM and non-medicated AAV-AD cohorts. (B) The male non-medicated AAV-AD cohort had significantly denser IBA1 than every other male cohort. Male AAV-AD cohorts had higher densities of GFAP in comparison to AAV-SHAM cohorts. n = 5-8. * = $p \leq 0.05$, ** = $p \leq 0.01$, *** = $p \leq 0.001$, **** = $p \leq 0.0001$.

Figure 12 shows images of IHC staining for non-neuronal cells. Figure 12A demonstrates positive staining for IBA1 with Figure 12B showing an enlarged image. Figure 12C demonstrates positive staining for GFAP with Figure 12D showing an enlarged image. Both cell types can be identified by the dark globular nucleus with thin wiry arms stretching out. Differences in the presence of microglia and astrocytes suggest the AAV-AD vector enhances the activation of non-neuronal cells in female mice. However, the male medicated cohorts appeared to have less microglia and more astrocytes when compared to non-medicated cohorts with the same vector, supporting a drug cocktail effect on activated astrocytes.

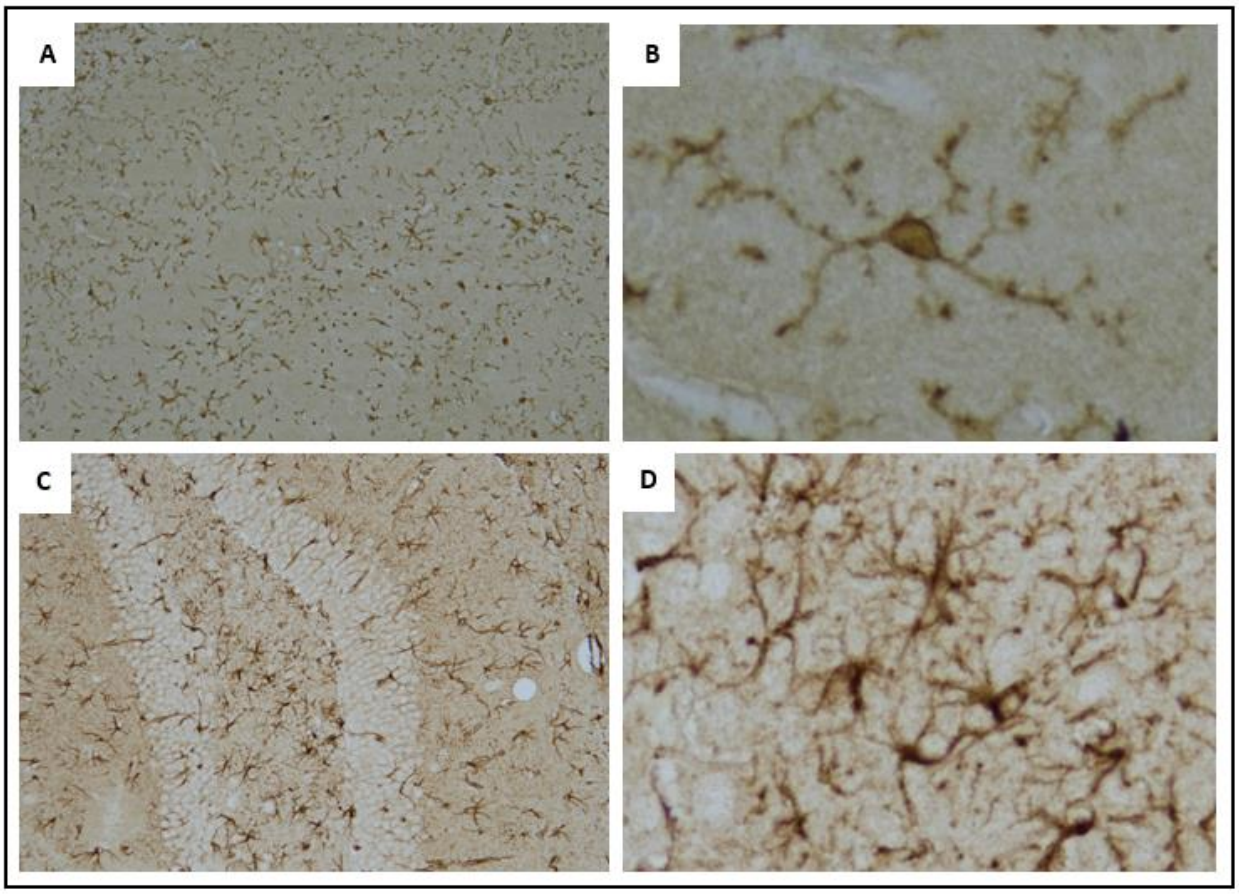

Figure 12. Images are representative of the characteristic markers of non-neuronal microglia and astrocytes in the hippocampus. (A) 20x image of the hippocampus, stained for microglia using IBA1 antibody. (B) Enhanced image of 12A. (C) 20x image of the hippocampus, stained for astrocytes using GFAP antibody. (D) Enhanced image of 12C.

The drug cocktail reduced the presence of age-related brain lesions in female mice infected with the AAV-AD vector.

Geropathology scores of age-related lesions are used to assess histopathological changes with increasing age in animal tissues and have been well established and documented for their value in assessing aging in mouse models (Synder 2019, Klug 2021). Female medicated cohorts on average had lower CLS scores than non-medicated cohorts regardless of infection with vector. The medicated AAV-AD cohort and the non-medicated AAV-AD cohort had a significant difference in age-related lesion score (Figure 13A). Surprisingly, male medicated cohorts had higher average scores in comparison to their non-medicated counterparts. Male cohorts also had higher averages for AAV-AD cohorts in comparison to AAV-SHAM cohorts (Figure 13B). These observations suggest that the drug cocktail delays progression of brain aging in females with or without early-stage AD.

Figure 14 shows images of H&E-LFB slides with annotations representing selected age-related lesion categories graded. Figure 14A demonstrates inflammation denoted by focal mononuclear inflammatory cell aggregates within the meninges. Figures 14B and 14C show thalamic and brain stem mineralization respectively, denoted by irregular amorphous purple to blue deposits. Figure 14D shows intraneuronal inclusion bodies denoted by amorphous eosinophilic inclusions within thalamic neurons.

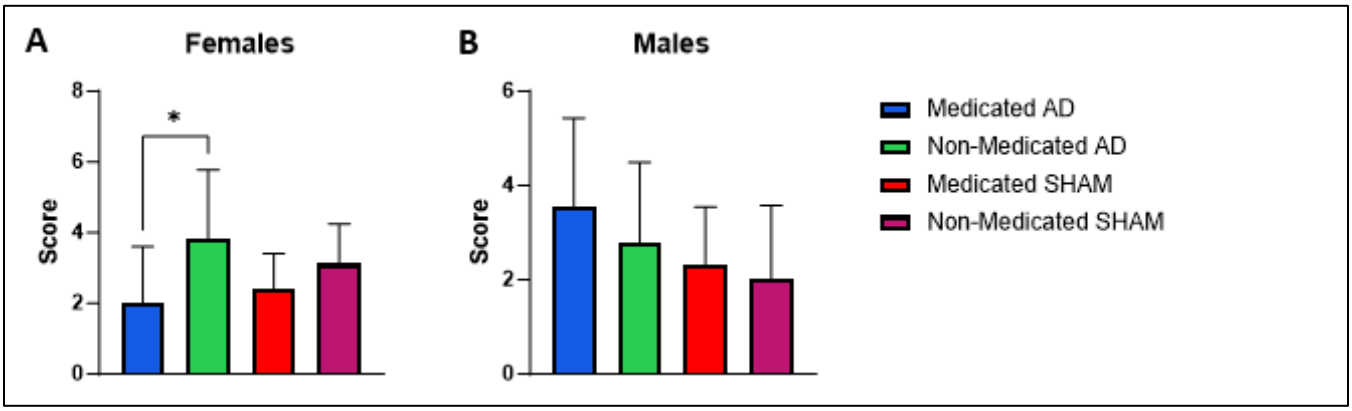

Figure 13. Geropathology grades for age-related lesions in the brain. (A) Female AAV-AD cohorts saw a significant decrease in age related lesions when treated with the drug cocktail. Medicated cohorts averaged lower scores in comparison to non-medicated cohorts. (B) Male AAV-AD cohorts on average had higher scores than AAV-SHAM cohorts. For all cohorts n = 5-8. * = $p \leq 0.05$.

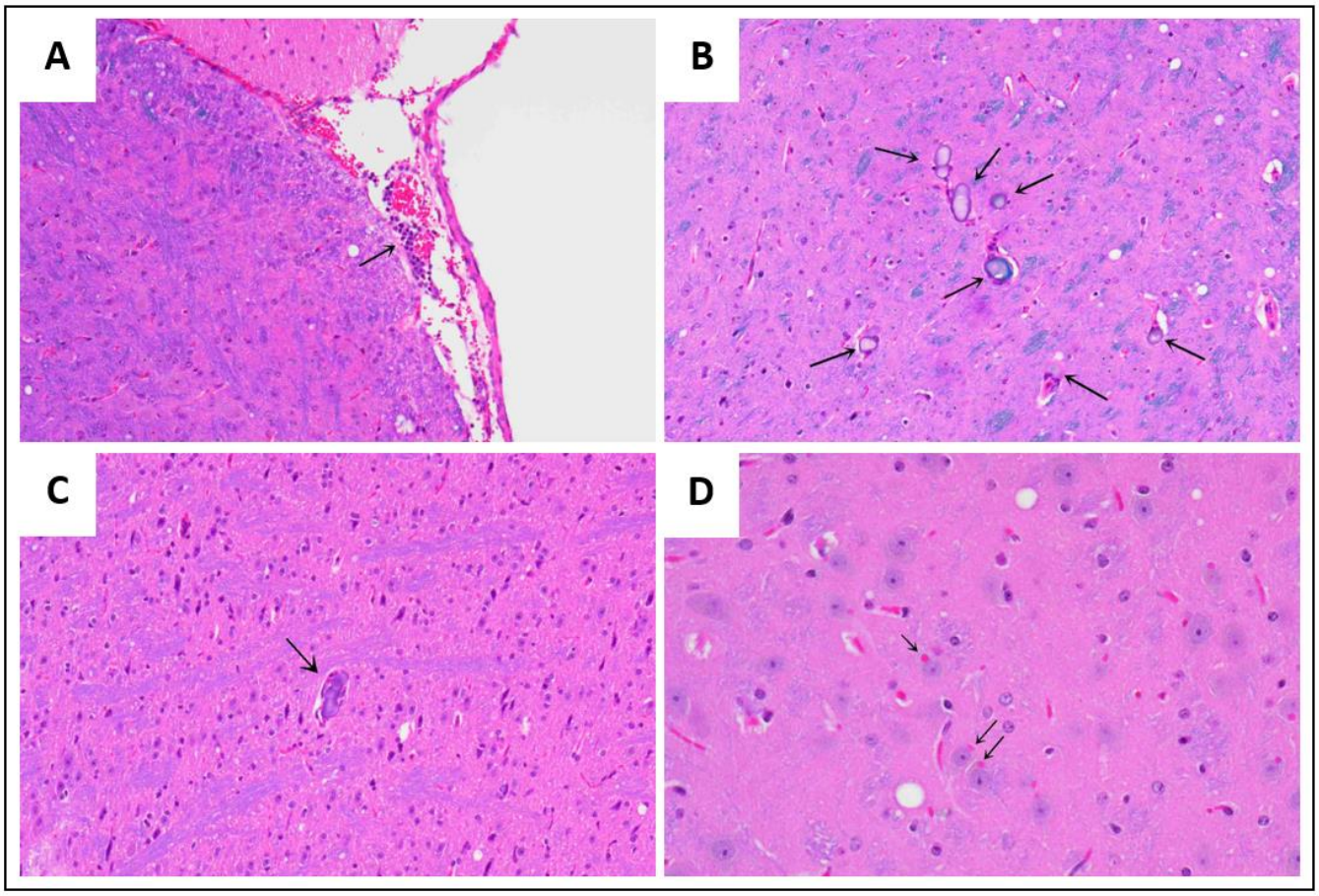

Figure 14. H&E-LFB stains with annotations of examples of age-related lesions in mouse brains. Black arrows point to specific examples. (A) Focal inflammation, meninges, 20x. (B) Multifocal thalamic mineralization, 20x. (C) Focal brain stem mineralization, 20x. (D) Thalamus, intraneuronal inclusion bodies, 40x.

Associations with inflammation and autophagy appeared to be mediated by the drug cocktail in both male and female cohorts.

Figures 15 and 16 contain correlation matrices comparing neuropathology, geropathology scores, and box maze cognition data to draw connections based on variable distribution within the data sets. Associations were considered strong if the Pearson correlation coefficient was less than or equal to -0.5 and greater than or equal to +0.5.

For female non-medicated cohorts (Figure 15A), a negative strong association was seen between cognitive impairment and both autophagy and microglia. Age-related lesions had strong positive associations with tau, inflammation, and autophagy. Aβ-42 density had strong positive associations with tau and inflammation. Tau had strong positive associations with inflammation and autophagy. Post synaptic integrity had strong negative associations with inflammation and autophagy. Lastly, inflammation had a strong positive association with autophagy. For female medicated cohorts in Figure 15B, cognitive impairment had a strong positive association with Aβ-42 and DNA damage. Age-related lesions had a strong positive association with autophagy and microglia. Aβ-42 had strong positive associations with tau and astrocytes. Tau had strong positive associations with astrocytes and strong negative associations with microglia. Presynaptic integrity had strong positive associations with autophagy. Postsynaptic integrity had a strong negative association with microglia. Lastly, inflammation had a strong positive association with DNA damage.

In the non-medicated cohorts (Figure 15B), the most influential variables seemed to be inflammation, autophagy, and tau. In the medicated cohorts the most influential variables seemed to be Aβ-42, tau, and microglia. This suggests the drug cocktail has relieved the burden of inflammation and autophagy, while increasing the activation of astrocytes in relation to Aβ-42 and tau, which seem to have a stronger influence over cognitive impairment.

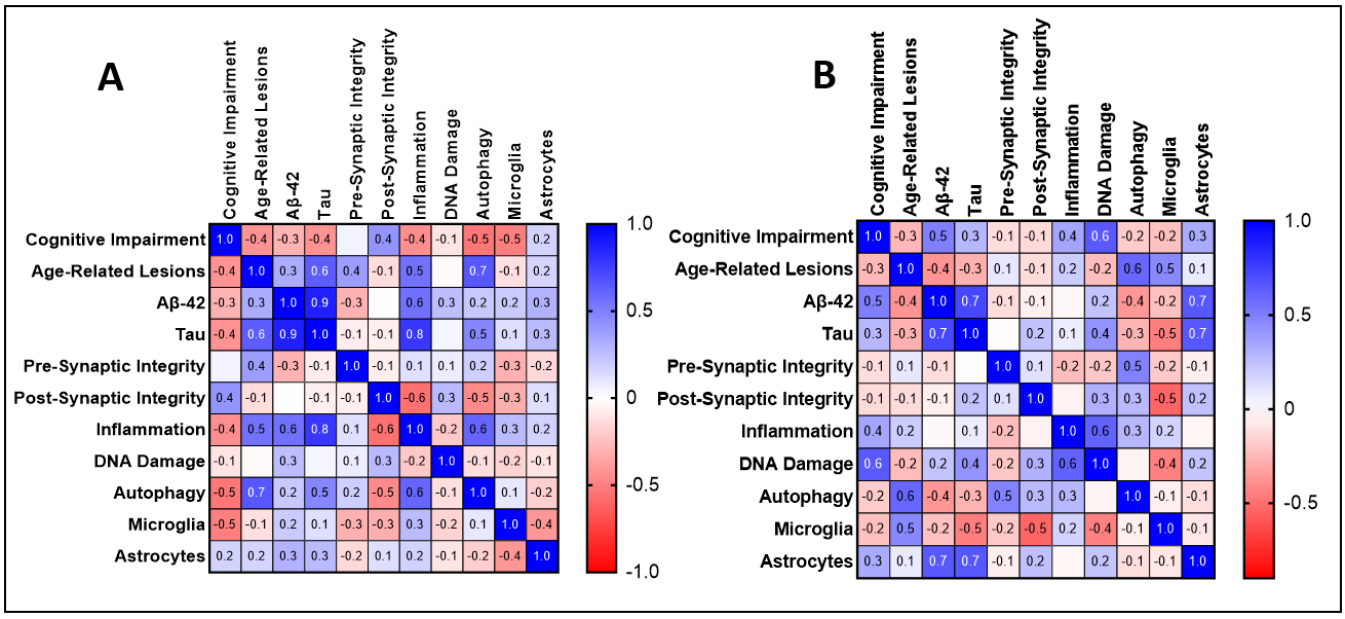

Figure 15. Females. Associations between neuropathology, age-related lesions, and cognitive impairment. Numbers shown are Pearson correlation coefficients. (A) Female non-medicated cohorts show the strongest influence from inflammation, autophagy, and tau. (B) Female medicated cohorts show strong influence from Aβ-42, tau, and microglia. Strong trend set at coefficient ≥ |0.5|. n = 14-15.

For male non-medicated cohorts (Figure 16A), box maze had strong negative associations with presynaptic integrity and inflammation. Aβ-42 had a strong positive association with tau. Tau had a strong positive association with inflammation. Pre-synaptic integrity had a strong negative association with microglia.

Inflammation had a strong positive association with autophagy. DNA damage had a strong positive association with autophagy. Lastly, autophagy had a strong positive association with microglia. For male medicated cohorts (Figure 16B), cognitive impairment had a strong negative association with Aβ-42. Age-related lesions had a positive association with microglia. Aβ-42 had a strong association with microglia. Tau had a strong association with DNA damage. Lastly, presynaptic integrity had a strong negative association with inflammation.

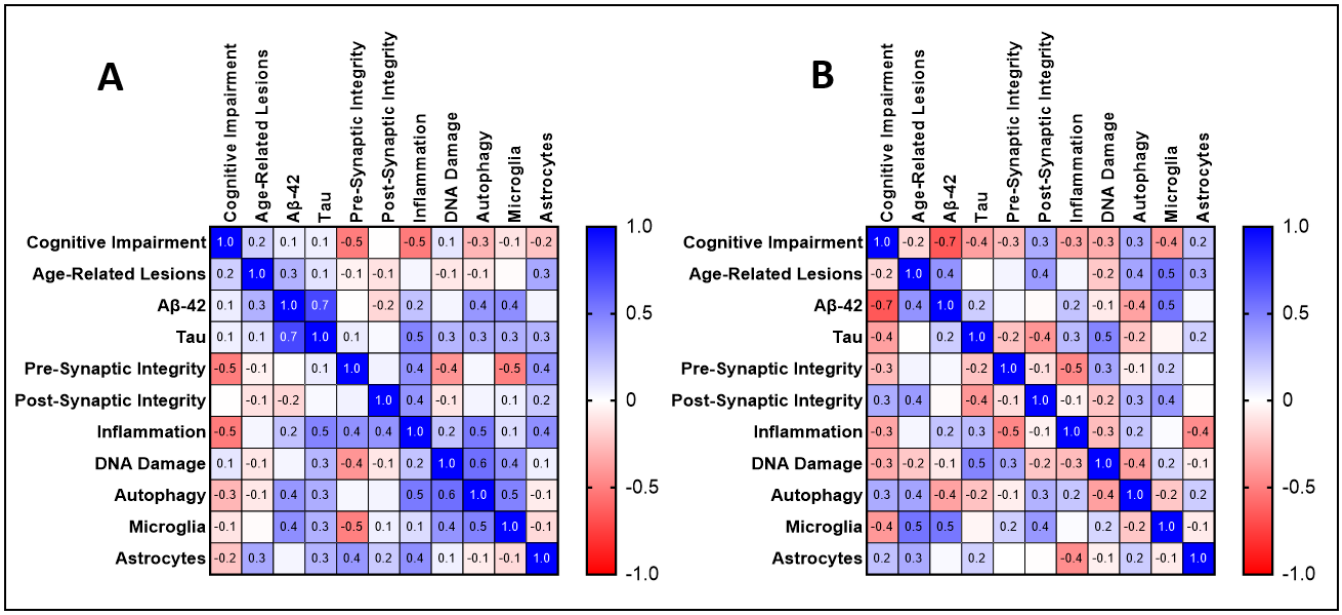

Figure 16. Males. Associations between neuropathology, age-related lesions, and cognitive impairment. Numbers shown are Pearson correlation coefficients. (A) Male non-medicated cohorts show the strongest influence from inflammation, autophagy, and microglia. (B) Male medicated cohorts show strong influence from Aβ-42, age-related lesions, and microglia. Strong trend set at coefficient ≥ |0.5|. n = 14-15.

In the non-medicated cohorts, the most influential variables seemed to be inflammation, autophagy, and microglia. In the medicated cohorts, the most influential variables seemed to be age-related lesions, Aβ-42, microglia. This suggests that while the drug cocktail can reduce the burden of inflammation and autophagy in male mice, cognitive impairment may be due to confounding factors outside the explored pathways.

Discussion

Metabolic effects of the drug cocktail. It has previously been reported that female and male C57BL/6 mice treated with a drug cocktail of rapamycin, acarbose, and phenylbutyrate had an associated loss of weight with a matching trend in body fat mass (Jiang 2022). In longitudinal mouse studies, weight gain in male and female mice has been reported to increase as late as 22 months of age (Yanai 2021). AD has been associated with weight loss and the presence of Aβ-42 and its correlation with neuroinflammation has been a proposed mechanism for the inflammation's effect on appetite (Sergi 2013, Sieske 2019). Additionally, frailty assessment in aging C57BL/6 mice has shown regardless of sex, frail mice had higher body weights and higher percentages of body fat which correlated with decreased endurance, slower walking speed, and less running wheel activity. Frail mice were also found to have decreased average lifespans (Baumann 2019). For female and male medicated cohorts, significant weight loss was observed in comparison to non-medicated cohorts which had non-significant weight loss over the study. It was also observed AAV-SHAM cohorts consumed more food on average compared to AAV-AD mice, indicating the drug cocktail may help to maintain body weight relative to the AAV-SHAM cohort. In addition, medicated cohorts had less fat mass prior to injection of the vector and at endpoint, apart from the

male non-medicated AAV-SHAM cohort. Together, these trends suggest the drug cocktail improves body composition for both male and female mice, but preferentially in female mice.

Jiang also reported no significant difference in the consumption of the medicated feed (2022). Figure 3E-3F demonstrates a significant difference in consumption of the medicated feed regardless of vector injection. One of the hallmarks of aging is insulin resistance and poor glucose response. Acarbose prevents glucose absorption in the small intestine and rapamycin inhibits the mTOR pathway activated by glucose and their effects have been compared to caloric restriction (Harrison 2014, Blagosklonny 2019). Rapamycin has additionally been reported to increase energy expenditure (Makki 2014). Due to the activity of these drugs, the difference seen in consumption makes sense for medicated cohorts in that greater consumption would be seen to introduce more nutrients and reclaim homeostasis (Augustine 2020). Differences between consumption may also occur from a longer period of consuming the diet and the increased age of the cohorts.

Overall, any changes in body weight and fat mass align with findings in previous studies but prolonged exposure to the drug cocktail for mice past 22 months of age has not yet been characterized to the author's knowledge. Additionally, this study demonstrates a robust impact of treatment with the drug cocktail on female cohorts and more subtle effect on male cohorts.

Cognitive Impairment. The box maze assay has been validated for its ability to assess learning impairment in aging mice (Mukherjee 2019, Darvas 2020). It was previously reported that the drug cocktail reduced learning impairment in comparison to control cohorts (Jiang 2022). Female cohorts on average performed better in the box maze in comparison to male cohorts. In the separation of fast and slow learners for each cohort, it can be seen medicated slow learners on average performed faster than non-medicated slow learners. In addition, medicated fast learners performed faster than non-medicated fast learners with the same vector (Figure 4A-4C). In male cohorts, AAV-SHAM fast learners performed faster than AAV-AD fast learners. Surprisingly, the non-medicated AAV-SHAM cohort performed the fastest comparing their fast and slow learners against the other cohorts (Figure 4B-4D). In addition, the separation of fast and slow learners reveals a much more robust difference in performance for female cohorts than it does for male cohorts.

This is surprising as Jiang also reported faster escape times for male cohorts in comparison to female cohorts (2022) and it has been reported female mice specifically encounter spatial cognitive impairment earlier than males (Benice 2006). Treatment with rapamycin and acarbose has been shown to be effective if administered in mid- or late-life in mice (Herrera 2023). It was seen when normalizing food intake to body weight, male cohorts in comparison to their respective female cohorts, consumed significantly less food in the final four weeks before endpoint regardless of diet. In comparison of non-medicated male and female cohorts, food consumption normalized to body weight should be equivalent. The cognitive impairment phenotype may then be due to factors outside the primary anatomic region of analysis selected in this study (hippocampus). Regardless, the model still reflects the impact of the cocktail on cognitive impairment and suggests a vector dependent effect on performance.

Expression of Aβ-42 and Tau. Alzheimer's disease is a global disease of the human brain. However, the hippocampus is one of the first regions of the brain to show histopathological evidence of AD. Early-stage AD is characterized by mild cognitive impairment and the accumulation and aggregation of Aβ-42 and tau protein (Braak 1991). For this reason, the hippocampus was chosen to analyze the model. Green Fluorescent Protein (GFP) was included in the Aβ-42 construct as a reporter gene to indirectly validate the induction of the viral vector. For both male and female AAV-AD cohorts, density of positive expression of GFP was specific and significant in comparison to AAV-SHAM cohorts. Moreover, no differences were observed between the density of

GFP in the hippocampus between the medicated and non-medicated cohorts. This comparison acted as a control for the potential effects of the drug cocktail on the vector.

In determining the expression of the human Aβ-42 sequence induced by the vector, the H31L21 antibody was chosen for its specificity. The commonly used antibody to detect Aβ pathology in human brains, 6E10, binds generally to amyloid proteins and demonstrated artifact cross reactivity when used in mouse brains. Female AAV-AD cohorts had significant in expression of Aβ-42 over AAV-SHAM cohorts regardless of diet, and the female medicated AAV-AD had a significant decrease in density compared to the non-medicated AAV-AD cohort. While AAV-AD specific density was seen in male cohorts, there was not a significant difference between the medicated and non-medicated AAV-AD cohort. This difference not only demonstrates the ability for the vector to enhance resilience to AD Aβ-42 accumulation, but also mirrors the reduction in cognitive impairment seen in the box maze. Common markers for phosphorylated tau such as AT8 and serine-404 target conserved sequences in mice. HT7 targets a sequence specific for human tau regardless of phosphorylation and so HT7 was chosen for human tau detection. Due to the only human tau sequence in the AAV-AD cohorts coming from the construct, specific staining was able to be achieved. Female AAV-AD cohorts saw significant and specific density of tau in comparison to AAV-SHAM cohorts. While on average male AAV-AD cohorts had specific density of tau, the differences between the AAV-SHAM cohorts were not significant. Additionally male AAV-AD cohorts had half the tau density of AAV-AD female cohorts. This could be due to several AAV-AD males containing densities equivalent to their AAV-SHAM counterparts. Considering the viral vector used was the same for Aβ-42 and tau, and that male mice do seem to have higher levels of autophagy in comparison to female mice, it is possible an autophagic specificity for tau is present in male cohorts. It has previously reported tau is degraded via autophagy while current research on Aβ-42 clearance focuses on extra-cellular aggregates (Hamano 2021, Wei 2019, Bharadwaj 2020).

Overall, neuronal infection with the AAV-AD vector mediated specific and significantly higher density of protein expression of Aβ-42 and tau in the hippocampus of mice compared to the AAV-SHAM cohorts. Expression of Aβ-42 and tau demonstrates expression within neurons (Figure 4) indicating an early-stage model of AD, as later stages are characterized by extracellular Aβ-42 aggregates, not seen during pathologist review of H&E-LFB slides.

Neuropathology and Non-Neuronal Cells. The progression of AD even in the early stages affects multiple processes resulting in a more severe “aging” phenotype. One of the first affected pathways tied closely with the onset of mild cognitive impairment is synaptic integrity. It has been suggested that soluble Aβ-42 causes synaptic dysfunction prior to the formation of plaques and clinical detection (Solkoe 2002, John 2022). In female medicated cohorts, increased levels of synaptophysin were seen when compared to non-medicated cohorts. In addition, increased levels of PSD-95 were also seen in medicated cohorts when compared to non-medicated cohorts of the same vector. In comparison with the AAV-AD and AAV-SHAM cohorts, synaptophysin and PSD-95 were decreased in AAV-AD cohorts relative to the respective AAV-SHAM cohorts. These results suggest the drug cocktail improves synaptic integrity, while the presence of AAV-AD proteins harm synaptic integrity. These findings are mirrored in the box maze data where the female medicated AAV-SHAM cohort showed less learning impairment. Male cohorts saw similar trends, with a smaller difference in synaptophysin between AAV-AD cohorts and greater expression of PSD-95 in non-medicated cohorts. The drug cocktail appears to enhance synaptophysin expression in medicated mice but not the expression in PSD-95. It has been previously found that PBA reduces cognitive impairment and increased synaptic plasticity in mouse models of AD (Ricobaraza 2009, Wiley 2011). Male non-medicated cohorts seem to have higher densities of PSD-95 and synaptophysin in comparison to female non-medicated cohorts. Given the greater burden of Aβ-42 in non-medicated female mice, the findings of the study may suggest these changes are driven by AD proteins, though the differences in box maze suggest synaptic integrity across sexes is dependent on more than synaptophysin and PSD95.

The buildup of Aβ-42 and tau protein aggregates can cause neuronal injury through accumulated double strand breaks (Shanbhag 2019) and a vicious cycle of pro-inflammatory cytokines (Sinyor 2020). Additionally, these increases activate an autophagic response which has been reported to clear Aβ-42 in mouse models of AD (Heckmann 2019). For both male and female cohorts, medicated cohorts had less inflammation in comparison to non-medicated cohorts with the same vector, however, the non-medicated AAV-AD cohort had a much more substantial level of inflammation. Overall, it does appear the male cohorts have higher levels of inflammation in comparison to the female cohorts. The drug cocktail has previously been validated for its ability to reduce inflammation in major systemic organs as well as in the brain (Jiang 2022, 2023) matching our study results. The level of inflammation suggests an AAV-AD specific instigation of inflammation and the drug cocktail's ability to modulate that response. Female AAV-AD cohorts had more DNA damage in comparison to their AAV-SHAM counterparts and medicated cohorts had less DNA damage in comparison to non-medicated cohorts. The male medicated AAV-AD cohort has less DNA damage than the non-medicated cohorts, however the medicated AAV-SHAM cohort had more DNA damage than the non-medicated AAV-SHAM cohort. The male cohort again has a lower burden of Aβ-42 in the brain and lower protein aggregation in the neurons may reduce neuronal injury in the medicated cohort. Additionally, the non-medicated AAV-SHAM performed well in the box maze suggesting less progressive DNA damage may contribute to its faster learning times. In female cohorts, autophagy was increased in for the medicated AAV-SHAM cohort in comparison to the non-medicated AAV-SHAM cohort, but this trend was inverted for AAV-AD cohorts. In males, non-medicated cohorts had higher levels of autophagy in comparison to medicated cohorts. Female cohorts did see a significant decrease in Aβ-42 expression which may explain the decrease in autophagy for the medicated AAV-AD cohort. Males see the inversion of what is expected, though autophagy does mirror trends in PSD95 which may indicate opposing sex differences in hippocampal health.

Microglia and astrocytes are controversial for their role in AD pathogenesis. While microglia help to degrade Aβ-42, they also participate in the release pro-inflammatory cytokines which activate astrocytes, preventing them from supporting synapse plasticity and maintenance (Liddelow 2017) as well as participating in synapse loss through engulfment (Hansen 2018). Astrocytes participate in synapse maintenance, regulation of the inflammatory response and provide neurons with nutrients but hyperproduce hydrogen peroxide and atrophy as AD progresses (Chun 2020). In our study, female medicated cohorts had increased levels of microglia in comparison to non-medicated cohorts. Male cohorts had the opposite trend where medicated cohorts had less activated microglia expression in comparison to non-medicated cohorts with the same vector. For male cohorts, the trends in microglia mirror autophagy, suggesting the levels of autophagy seen may be activated by microglia. The female cohorts demonstrated the opposite trend of what was expected. It is possible microglia, in combination with a reduction in inflammation, lead to more effective response to increases in Aβ-42, which would explain increases in microglia and trends in Aβ-42 expression for male and female cohorts. In female cohorts, astrocytes have increased density in medicated cohorts when compared against non-medicated cohorts. Male mice show a mirrored trend within cohorts of the vector. Activation of microglia in females could be the reason for the activation of astrocytes as the trends are mirrored across cohorts. As previously stated, sex differences in the activation response of astrocytes may explain the differences between non-medicated cohorts. Trends for astrocytes in male cohorts more closely mirror the trends for presence and severity of age-related lesions in the brain.

Overall, the drug cocktail appeared to rescue AAV-AD inflicted degeneration of synaptic integrity, increased inflammation and DNA damage, and enhance healthy microglia-neuron interactions.

Geropathology. The geropathology grading platform is a standardized assessment of age-related lesions in tissues through numerical grade scores associated with increased severity. Standard curves have been created and validated in mice to demonstrate the ability of the platform to assess aging (Synder 2019, Klug 2021).

Previously, Jiang reported a decrease in geropathology scores for the main body organs of drug cocktail medicated mice (2022). Geropathology scores for brains from aged mice have not previously been reported for the drug cocktail. In female mice, brains from medicated cohorts had lower geropathology scores in comparison to non-medicated cohorts with the medicated AAV-AD cohort having a significant decrease in geropathology score in comparison to the non-medicated AAV-SHAM cohort. In contrast, male medicated cohorts had higher geropathology scores in comparison to the non-medicated cohorts with the same vector. These observations indicate that the drug cocktail increased resilience to aging in the brains of female mice, but not in the brains of male mice. The trends in geropathology scores mirrored trends in astrocytes. With increasing age, astrocytes become unable to carry out their normal functions and become reactive, as they would in AD (Clarke 2017). GFAP, the marker used for astrocytes, increases when astrocytes become reactive. It is possible that astrocytes have a direct impact on age-related lesions in the brain caused by natural aging, especially in old mice at 27 months of age.

Overall, female mice appeared to have a robust benefit from the drug cocktail on age-related lesions in comparison to male mice who appeared to have little to no benefit. While there was no reduction in geropathology score between medicated and non-medicated cohorts, the averages for both the AAV-AD infected cohorts were higher than the averages for the AAV-SHAM infected cohorts. In addition, the non-medicated AAV-SHAM cohort performed uniquely well against expectations, which is supported in the neuropathology data. Aside from this, the male and female medicated cohorts had nearly identical scores. With an increase in astrocyte activation in male AAV-AD infected cohorts and in combination with more inflammation in comparison to female cohorts, it is possible activated astrocytes are contributing to vacuolation and mineralization in the brain (Mattson 2003, Chen 2015). With these differences, it is clear between astrocyte activation and in addition, for AAV-AD infected mice, Aβ-42 expression matched with geropathology scoring. Together, this may indicate an effect of AAV-AD induced proteins to modulate astrocyte activation and, in turn, the presence of age-related lesions. It also further demonstrates the ability of the drug cocktail to preferentially benefit AAV-AD in female mice.

Associations. For non-medicated females, autophagy activated by microglia was most likely responsible for faster box maze times resulting in the negative associations. The strong positive associations for geropathology are likely due to the increase in tau leading to an inflammatory response and the necessity for autophagy all the while increasing the presence of age-related lesions. Aβ-42 and tau associating strongly implies consistent relative expression of both proteins and the association of both with inflammation implies specific responses to the AAV-AD vector. Postsynaptic integrity had negative associations with inflammation and autophagy likely as a response to production of inflammatory proteins and the necessity to degrade excess proteins. These associations demonstrate the wide necessity of autophagy and the far-reaching impact of inflammation in response to the AD protein expression.

In contrast, female medicated cohorts demonstrate positive associations with Aβ-42 and DNA damage are the driving factors for box maze, with DNA damage associating with inflammation. The overall reduction in inflammation is likely from a reduction in expression of Aβ-42, with inflammation arising from DNA damage instead. Mice with less Aβ-42 and DNA damage then perform better in the box maze. Geropathology score is still strongly associated with autophagy, likely induced by microglia. Aβ-42 and tau have consistent relative expression as well as a strong association with activated astrocytes. The association with activated astrocytes may be a compensatory measure against an increase in tau as it appears tau and microglia have a strong negative relationship. These associations suggest that Aβ-42 and tau play a role in the activation of astrocytes.

Between the non-medicated and medicated females, differences induced by the medicated diet are revealed. Non-medicated female cohorts have much greater amounts of inflammation and upregulation of autophagy

induced by Aβ-42 and tau. In contrast, medicated mice over all do not have the same up-regulation of inflammation and autophagy but do display an increase in synaptic integrity as well as active astrocyte association with Aβ-42 and tau expression. The drug cocktail thus demonstrates mediation of synaptic integrity, inflammation, and autophagy within the female model.

Box maze in male non-medicated cohorts had strong negative associations with presynaptic integrity and inflammation. Tau had strong associations with Aβ-42, implying consistent relative expression, and inflammation. Inflammation and autophagy induced by microglia had a strong association as a response to AAV-AD protein expression. Lastly, microglia had a strong negative association with presynaptic integrity, possible due to engulfment of synapses. These associations suggest an inflammatory cascade response to the AAV-AD vector ending in cognitive impairment.

Medicated males had a strong negative association with Aβ-42 and box maze. This is a counter intuitive relationship. Microglia have a strong association with geropathology scores and Aβ-42. There does not seem to be astrocyte activation and so microglia carry the burden for the residual inflammation caused by Aβ-42. Tau had a strong association with DNA damage, and presynaptic integrity had a strong negative association with inflammation. These associations imply Aβ-42 induces a microglia response that impacts age-related lesions accordingly. Due to the similarity in the box maze, it appears in the medicated cohorts there is no effect of the AAV-AD on box maze performance.

The differences between the males demonstrate small effects of the drug cocktail. Similar to the female cohorts, the drug cocktail does reduce inflammation, autophagy, and improves synaptic integrity. However, it does not appear like in the female cohorts, improvement of synaptic integrity results in a reduction of cognitive impairment. This could be due to additional variables outside the hippocampus impacting overall performance.

In an evaluation of the model, resilience to aging was enhanced in male and female mice primarily in pathways of autophagy, synaptic integrity, and inflammation, with a much bigger increase to resilience seen in female mice. While cognitive impairment appeared to be subtle, Alzheimer's disease is a disease of slow progression where clinical phenotypes present after neuropathology has been well established. Additionally, the drug cocktail significantly delayed the onset of age-related lesions in the brain and the presence of Aβ-42 in female mice. It is important to note the effects seen in this study were analyzed as a combination of all three drugs and individual drugs were not tested in this study. Jiang et al. demonstrated a stronger effect in increasing resilience in mouse brains for the combination of drugs (2023). More in depth analysis of specific downstream targets and pathways of each drug included in the cocktail would need to be evaluated for determining their contribution to the results. In addition, while young controls have been used in the past to validate the effects of the drug cocktail (Jiang 2023), a control cohort of mice not infected with either vector may help to elucidate a baseline of aging pathology and injection effect within the AAV cohorts. All cohorts in this study were infected with an AAV vector, so any plausible effect of the virus would be controlled for. This model of early-stage Alzheimer's disease is a valuable research tool not only for exploratory research but also for evaluation of AD expression within the context of aging.

In conclusion, female mice were more susceptible to the early development of AD neuropathology and learning impairment, and more responsive to treatment with the drug cocktail in comparison to male mice. Translationally, a model of AD where females are more susceptible would have greater value as women have a greater burden and incidence of disease compared to men. Future studies will look to establish genetic tests for biological aging and similar in-depth analysis of neuropathology in additional regions of the brain.

References

Ainslie A, Huiting W, Barazzuol L, Bergink S. Genome instability and loss of protein homeostasis: converging paths to neurodegeneration? Open Biol. 2021 Apr;11(4):200296. doi: 10.1098/rsob.200296. Epub 2021 Apr 21. PMID: 33878947; PMCID: PMC8059563.

Alhurani RE, Vassilaki M, Aakre JA, Mielke MM, Kremers WK, Machulda MM, Geda YE, Knopman DS, Petersen RC, Roberts RO. Decline in Weight and Incident Mild Cognitive Impairment: Mayo Clinic Study of Aging. JAMA Neurol. 2016 Apr;73(4):439-46. doi: 10.1001/jamaneurol.2015.4756. Erratum in: JAMA Neurol. 2017 Mar 1;74(3):364. PMID: 26831542; PMCID: PMC4828256.

Augustine V, Lee S, Oka Y. Neural Control and Modulation of Thirst, Sodium Appetite, and Hunger. Cell. 2020 Jan 9;180(1):25-32. doi: 10.1016/j.cell.2019.11.040. PMID: 31923398; PMCID: PMC7406138.

Bamia C, Halkjaer J, Lagiou P, Trichopoulos D, Tjønneland A, Berentzen TL, Overvad K, Clavel-Chapelon F, Boutron-Ruault MC, Rohrmann S, Linseisen J, Steffen A, Boeing H, May AM, Peeters PH, Bas Bueno-de-Mesquita H, van den Berg SW, Dorronsoro M, Barricarte A, Rodriguez Suarez L, Navarro C, González CA, Boffetta P, Pala V, Hallmans G, Trichopoulou A. Weight change in later life and risk of death amongst the elderly: the European Prospective Investigation into Cancer and Nutrition-Elderly Network on Ageing and Health study. J Intern Med. 2010 Aug;268(2):133-44. doi: 10.1111/j.1365-2796.2010.02219.x. Epub 2010 Jan 28. PMID: 20210842.

Baumann CW, Kwak D, Thompson LV. Sex-specific components of frailty in C57BL/6 mice. Aging (Albany NY). 2019 Jul 29;11(14):5206-5214. doi: 10.18632/aging.102114. PMID: 31355774; PMCID: PMC6682513.

Benice TS, Rizk A, Kohama S, Pfankuch T, Raber J. Sex-differences in age-related cognitive decline in C57BL/6J mice associated with increased brain microtubule-associated protein 2 and synaptophysin immunoreactivity. Neuroscience. 2006;137(2):413-23. doi: 10.1016/j.neuroscience.2005.08.029. Epub 2005 Dec 5. PMID: 16330151.

Bharadwaj PR, Martins RN. Autophagy modulates Aβ accumulation and formation of aggregates in yeast. Mol Cell Neurosci. 2020 Apr;104:103466. doi: 10.1016/j.mcn.2020.103466. Epub 2020 Jan 18. PMID: 31962153.

Blagosklonny MV. Rapamycin for longevity: opinion article. Aging (Albany NY). 2019 Oct 4;11(19):8048-8067. doi: 10.18632/aging.102355. Epub 2019 Oct 4. PMID: 31586989; PMCID: PMC6814615.

Braak H, Braak E. Neuropathological stageing of Alzheimer-related changes. Acta Neuropathol. 1991;82(4):239-59. doi: 10.1007/BF00308809. PMID: 1759558.

Chen A, Akinyemi RO, Hase Y, Firbank MJ, Ndung'u MN, Foster V, Craggs LJ, Washida K, Okamoto Y, Thomas AJ, Polvikoski TM, Allan LM, Oakley AE, O'Brien JT, Horsburgh K, Ihara M, Kalaria RN. Frontal white matter hyperintensities, clasmatodendrosis and gliovascular abnormalities in ageing and post-stroke dementia. Brain. 2016 Jan;139(Pt 1):242-58. doi: 10.1093/brain/awv328. Epub 2015 Dec 14. PMID: 26667280; PMCID: PMC4905522.

Cho SJ, Lim HJ, Jo C, Park MH, Han C, Koh YH. Plasma ATG5 is increased in Alzheimer's disease. Sci Rep. 2019 Mar 18;9(1):4741. doi: 10.1038/s41598-019-41347-2. PMID: 30894637; PMCID: PMC6427023.

Chun H, Im H, Kang YJ, Kim Y, Shin JH, Won W, Lim J, Ju Y, Park YM, Kim S, Lee SE, Lee J, Woo J, Hwang Y, Cho H, Jo S, Park JH, Kim D, Kim DY, Seo JS, Gwag BJ, Kim YS, Park KD, Kaang BK, Cho H, Ryu H, Lee CJ. Severe reactive

astrocytes precipitate pathological hallmarks of Alzheimer's disease via H2O2- production. Nat Neurosci. 2020 Dec;23(12):1555-1566. doi: 10.1038/s41593-020-00735-y. Epub 2020 Nov 16. PMID: 33199896.

Clarke LE, Liddelow SA, Chakraborty C, Münch AE, Heiman M, Barres BA. Normal aging induces A1-like astrocyte reactivity. Proc Natl Acad Sci U S A. 2018 Feb 20;115(8):E1896-E1905. doi: 10.1073/pnas.1800165115. Epub 2018 Feb 7. PMID: 29437957; PMCID: PMC5828643.

Crespo-Castrillo A, Arevalo MA. Microglial and Astrocytic Function in Physiological and Pathological Conditions: Estrogenic Modulation. Int J Mol Sci. 2020 May 2;21(9):3219. doi: 10.3390/ijms21093219. PMID: 32370112; PMCID: PMC7247358.

Currais A, Fischer W, Maher P, Schubert D. Intraneuronal protein aggregation as a trigger for inflammation and neurodegeneration in the aging brain. FASEB J. 2017 Jan;31(1):5-10. doi: 10.1096/fj.201601184. PMID: 28049155; PMCID: PMC6191004.

Darvas M, Mukherjee K, Lee A, Ladiges W. A Novel One-Day Learning Procedure for Mice. Curr Protoc Mouse Biol. 2020 Mar;10(1):e68. doi: 10.1002/cpmo.68. PMID: 32096920.

Dewanjee S, Chakraborty P, Bhattacharya H, Chacko L, Singh B, Chaudhary A, Javvaji K, Pradhan SR, Vallamkondu J, Dey A, Kalra RS, Jha NK, Jha SK, Reddy PH, Kandimalla R. Altered glucose metabolism in Alzheimer's disease: Role of mitochondrial dysfunction and oxidative stress. Free Radic Biol Med. 2022 Nov 20;193(Pt 1):134-157. doi: 10.1016/j.freeradbiomed.2022.09.032. Epub 2022 Oct 4. PMID: 36206930.

Hamano T, Enomoto S, Shirafuji N, Ikawa M, Yamamura O, Yen SH, Nakamoto Y. Autophagy and Tau Protein. Int J Mol Sci. 2021 Jul 12;22(14):7475. doi: 10.3390/ijms22147475. PMID: 34299093; PMCID: PMC8303176.

Hansen DV, Hanson JE, Sheng M. Microglia in Alzheimer's disease. J Cell Biol. 2018 Feb 5;217(2):459-472. doi: 10.1083/jcb.201709069. Epub 2017 Dec 1. PMID: 29196460; PMCID: PMC5800817.

Harrison DE, Strong R, Allison DB, Ames BN, Astle CM, Atamna H, Fernandez E, Flurkey K, Javors MA, Nadon NL, Nelson JF, Pletcher S, Simpkins JW, Smith D, Wilkinson JE, Miller RA. Acarbose, 17-α-estradiol, and nordihydroguaiaretic acid extend mouse lifespan preferentially in males. Aging Cell. 2014 Apr;13(2):273-82. doi: 10.1111/acel.12170. Epub 2013 Nov 19. PMID: 24245565; PMCID: PMC3954939.

Heckmann BL, Teubner BJW, Tummers B, Boada-Romero E, Harris L, Yang M, Guy CS, Zakharenko SS, Green DR. LC3-Associated Endocytosis Facilitates β-Amyloid Clearance and Mitigates Neurodegeneration in Murine Alzheimer's Disease. Cell. 2019 Jul 25;178(3):536-551.e14. doi: 10.1016/j.cell.2019.05.056. Epub 2019 Jun 27. Erratum in: Cell. 2020 Dec 10;183(6):1733-1734. PMID: 31257024; PMCID: PMC6689199.

Herrera JJ, Pifer K, Louzon S, Leander D, Fiehn O, Day SM, Miller RA, Garratt M. Early or Late-Life Treatment With Acarbose or Rapamycin Improves Physical Performance and Affects Cardiac Structure in Aging Mice. J Gerontol A Biol Sci Med Sci. 2023 Mar 1;78(3):397-406. doi: 10.1093/gerona/glac221. PMID: 36342748; PMCID: PMC9977253.

Hu S, Yang T, Wang Y. Widespread labeling and genomic editing of the fetal central nervous system by in utero CRISPR AAV9-PHP.eB administration. Development. 2021 Jan 20;148(2):dev195586. doi: 10.1242/dev.195586. PMID: 33334860; PMCID: PMC7847274.

Jiang Z, Wang J, Imai D, Snider T, Klug J, Mangalindan R, Morton J, Zhu L, Salmon AB, Wezeman J, Hu J, Menon V, Marka N, Neidernhofer L, Ladiges W. Short term treatment with a cocktail of rapamycin, acarbose and

phenylbutyrate delays aging phenotypes in mice. Sci Rep. 2022 May 4;12(1):7300. doi: 10.1038/s41598-022-11229-1. PMID: 35508491; PMCID: PMC9067553.

John A, Reddy PH. Synaptic basis of Alzheimer's disease: Focus on synaptic amyloid beta, P-tau and mitochondria. Ageing Res Rev. 2021 Jan;65:101208. doi: 10.1016/j.arr.2020.101208. Epub 2020 Nov 4. PMID: 33157321; PMCID: PMC7770124.

Johnson SC, Rabinovitch PS, Kaeberlein M. mTOR is a key modulator of ageing and age-related disease. Nature. 2013 Jan 17;493(7432):338-45. doi: 10.1038/nature11861. PMID: 23325216; PMCID: PMC3687363.

Klug J, Christensen S, Imai DM, Snider TA, Ladiges W. The geropathology of organ-specific aging. J Transl Sci. 2021 Feb;7(1):458. doi: 10.15761/jts.1000458. Epub 2021 Jun 16. PMID: 34504718; PMCID: PMC8425292.

Konno A, Hirai H. Efficient whole brain transduction by systemic infusion of minimally purified AAV-PHP.eB. J Neurosci Methods. 2020 Dec 1;346:108914. doi: 10.1016/j.jneumeth.2020.108914. Epub 2020 Aug 15. PMID: 32810474.

Liddelow SA, Guttenplan KA, Clarke LE, Bennett FC, Bohlen CJ, Schirmer L, Bennett ML, Münch AE, Chung WS, Peterson TC, Wilton DK, Frouin A, Napier BA, Panicker N, Kumar M, Buckwalter MS, Rowitch DH, Dawson VL, Dawson TM, Stevens B, Barres BA. Neurotoxic reactive astrocytes are induced by activated microglia. Nature. 2017 Jan 26;541(7638):481-487. doi: 10.1038/nature21029. Epub 2017 Jan 18. PMID: 28099414; PMCID: PMC5404890.

Lin X, Kapoor A, Gu Y, Chow MJ, Peng J, Zhao K, Tang D. Contributions of DNA Damage to Alzheimer's Disease. Int J Mol Sci. 2020 Feb 28;21(5):1666. doi: 10.3390/ijms21051666. PMID: 32121304; PMCID: PMC7084447.

Makki K, Taront S, Molendi-Coste O, Bouchaert E, Neve B, Eury E, Lobbens S, Labalette M, Duez H, Staels B, Dombrowicz D, Froguel P, Wolowczuk I. Beneficial metabolic effects of rapamycin are associated with enhanced regulatory cells in diet-induced obese mice. PLoS One. 2014 Apr 7;9(4):e92684. doi: 10.1371/journal.pone.0092684. PMID: 24710396; PMCID: PMC3977858.

Mathiesen SN, Lock JL, Schoderboeck L, Abraham WC, Hughes SM. CNS Transduction Benefits of AAV-PHP.eB over AAV9 Are Dependent on Administration Route and Mouse Strain. Mol Ther Methods Clin Dev. 2020 Oct 20;19:447-458. doi: 10.1016/j.omtm.2020.10.011. PMID: 33294493; PMCID: PMC7683292.

Mattson MP, Chan SL. Neuronal and glial calcium signaling in Alzheimer's disease. Cell Calcium. 2003 Oct-Nov;34(4-5):385-97. doi: 10.1016/s0143-4160(03)00128-3. PMID: 12909083.

Mukherjee KK, Lee AY, Zhu L, Darvas M, Ladiges W. Sleep-deprived cognitive impairment in aging mice is alleviated by rapamycin. Aging Pathobiol Ther. 2019 Dec 30;1(1):5-9. doi: 10.31491/apt.2019.12.002. PMID: 35083443; PMCID: PMC8789090.

Orre M, Kamphuis W, Osborn LM, Jansen AHP, Kooijman L, Bossers K, Hol EM. Isolation of glia from Alzheimer's mice reveals inflammation and dysfunction. Neurobiol Aging. 2014 Dec;35(12):2746-2760. doi: 10.1016/j.neurobiolaging.2014.06.004. Epub 2014 Jun 14. PMID: 25002035.

Paganoni S, Macklin EA, Hendrix S, Berry JD, Elliott MA, Maiser S, Karam C, Caress JB, Owegi MA, Quick A, Wymer J, Goutman SA, Heitzman D, Heiman-Patterson T, Jackson CE, Quinn C, Rothstein JD, Kasarskis EJ, Katz J, Jenkins L, Ladha S, Miller TM, Scelsa SN, Vu TH, Fournier CN, Glass JD, Johnson KM, Swenson A, Goyal NA, Pattee GL, Andres PL, Babu S, Chase M, Dagostino D, Dickson SP, Ellison N, Hall M, Hendrix K, Kittle G, McGovern M, Ostrow

J, Pothier L, Randall R, Shefner JM, Sherman AV, Tustison E, Vigneswaran P, Walker J, Yu H, Chan J, Wittes J, Cohen J, Klee J, Leslie K, Tanzi RE, Gilbert W, Yeramian PD, Schoenfeld D, Cudkowicz ME. Trial of Sodium Phenylbutyrate-Taurursodiol for Amyotrophic Lateral Sclerosis. N Engl J Med. 2020 Sep 3;383(10):919-930. doi: 10.1056/NEJMoa1916945. PMID: 32877582; PMCID: PMC9134321.

Preman P, Alfonso-Triguero M, Alberdi E, Verkhratsky A, Arranz AM. Astrocytes in Alzheimer's Disease: Pathological Significance and Molecular Pathways. Cells. 2021 Mar 4;10(3):540. doi: 10.3390/cells10030540. PMID: 33806259; PMCID: PMC7999452.

Ricobaraza A, Cuadrado-Tejedor M, Pérez-Mediavilla A, Frechilla D, Del Río J, García-Osta A. Phenylbutyrate ameliorates cognitive deficit and reduces tau pathology in an Alzheimer's disease mouse model. Neuropsychopharmacology. 2009 Jun;34(7):1721-32. doi: 10.1038/npp.2008.229. Epub 2009 Jan 14. PMID: 19145227.

Posillico, C.K., Garcia-Hernandez, R.E. & Tronson, N.C. Sex differences and similarities in the neuroimmune response to central administration of poly I:C. J Neuroinflammation 18, 193 (2021). https://doi.org/10.1186/s12974-021-02235-7

Selkoe DJ. Alzheimer's disease is a synaptic failure. Science. 2002 Oct 25;298(5594):789-91. doi: 10.1126/science.1074069. PMID: 12399581.

Selvarani R, Mohammed S, Richardson A. Effect of rapamycin on aging and age-related diseases-past and future. Geroscience. 2021 Jun;43(3):1135-1158. doi: 10.1007/s11357-020-00274-1. Epub 2020 Oct 10. PMID: 33037985; PMCID: PMC8190242.

Sergi G, De Rui M, Coin A, Inelmen EM, Manzato E. Weight loss and Alzheimer's disease: temporal and aetiologic connections. Proc Nutr Soc. 2013 Feb;72(1):160-5. doi: 10.1017/S0029665112002753. Epub 2012 Oct 31. PMID: 23110988.

Schneider, C. A., Rasband, W. S., & Eliceiri, K. W. (2012). NIH Image to ImageJ: 25 years of image analysis. Nature Methods, 9(7), 671–675. doi:10.1038/nmeth.2089

Schorr A, Carter C, Ladiges W. The potential use of physical resilience to predict healthy aging. Pathobiol Aging Age Relat Dis. 2017 Nov 21;8(1):1403844. doi: 10.1080/20010001.2017.1403844. PMID: 29291035; PMCID: PMC5700501.

Shanbhag NM, Evans MD, Mao W, Nana AL, Seeley WW, Adame A, Rissman RA, Masliah E, Mucke L. Early neuronal accumulation of DNA double strand breaks in Alzheimer's disease. Acta Neuropathol Commun. 2019 May 17;7(1):77. doi: 10.1186/s40478-019-0723-5. PMID: 31101070; PMCID: PMC6524256.

Sieske L, Janssen G, Babel N, Westhoff TH, Wirth R, Pourhassan M. Inflammation, Appetite and Food Intake in Older Hospitalized Patients. Nutrients. 2019 Aug 22;11(9):1986. doi: 10.3390/nu11091986. PMID: 31443557; PMCID: PMC6770921.

Sinyor B, Mineo J, Ochner C. Alzheimer's Disease, Inflammation, and the Role of Antioxidants. J Alzheimers Dis Rep. 2020 Jun 16;4(1):175-183. doi: 10.3233/ADR-200171. PMID: 32715278; PMCID: PMC7369138.

Snyder JM, Snider TA, Ciol MA, Wilkinson JE, Imai DM, Casey KM, Vilches-Moure JG, Pettan-Brewer C, Pillai SPS, Carrasco SE, Salimi S, Ladiges W. Validation of a geropathology grading system for aging mouse studies.

Geroscience. 2019 Aug;41(4):455-465. doi: 10.1007/s11357-019-00088-w. Epub 2019 Aug 29. PMID: 31468322; PMCID: PMC6815299.

Strong R, Miller RA, Cheng CJ, Nelson JF, Gelfond J, Allani SK, Diaz V, Dorigatti AO, Dorigatti J, Fernandez E, Galecki A, Ginsburg B, Hamilton KL, Javors MA, Kornfeld K, Kaeberlein M, Kumar S, Lombard DB, Lopez-Cruzan M, Miller BF, Rabinovitch P, Reifsnyder P, Rosenthal NA, Bogue MA, Salmon AB, Suh Y, Verdin E, Weissbach H, Newman J, Maccchiarini F, Harrison DE. Lifespan benefits for the combination of rapamycin plus acarbose and for captopril in genetically heterogeneous mice. Aging Cell. 2022 Dec;21(12):e13724. doi: 10.1111/acel.13724. Epub 2022 Sep 30. PMID: 36179270; PMCID: PMC9741502.

Tarrant JC, Savickas P, Omodho L, Spinazzi M, Radaelli E. Spontaneous Incidental Brain Lesions in C57BL/6J Mice. Vet Pathol. 2020 Jan;57(1):172-182. doi: 10.1177/0300985819859878. Epub 2019 Jul 4. PMID: 31272300.

Ward JM, Vogel P, Sundberg JP. Brain and spinal cord lesions in 28 inbred strains of aging mice. Vet Pathol. 2022 Nov;59(6):1047-1055. doi: 10.1177/03009858221120009. Epub 2022 Sep 5. PMID: 36062914.

Wei Y, Zhou J, Wu J, Huang J. ERβ promotes Aβ degradation via the modulation of autophagy. Cell Death Dis. 2019 Jul 22;10(8):565. doi: 10.1038/s41419-019-1786-8. Erratum in: Cell Death Dis. 2019 Aug 23;10(9):634. PMID: 31332160; PMCID: PMC6646346.

Wiley JC, Pettan-Brewer C, Ladiges WC. Phenylbutyric acid reduces amyloid plaques and rescues cognitive behavior in AD transgenic mice. Aging Cell. 2011 Jun;10(3):418-28. doi: 10.1111/j.1474-9726.2011.00680.x. Epub 2011 Mar 22. PMID: 21272191.

Yanai S, Endo S. Functional Aging in Male C57BL/6J Mice Across the Life-Span: A Systematic Behavioral Analysis of Motor, Emotional, and Memory Function to Define an Aging Phenotype. Front Aging Neurosci. 2021 Aug 2;13:697621. doi: 10.3389/fnagi.2021.697621. PMID: 34408644; PMCID: PMC8365336.

Zhang L, Pitcher LE, Prahalad V, Niedernhofer LJ, Robbins PD. Targeting cellular senescence with senotherapeutics: senolytics and senomorphics. FEBS J. 2023 Mar;290(5):1362-1383. doi: 10.1111/febs.16350. Epub 2022 Feb 1. PMID: 35015337.